In vivo identification of GTPase interactors by mitochondrial relocalization and proximity biotinylation

Alison Gillingham[1]*, Jessie Bertram[1], Farida Begum and Sean Munro*

MRC Laboratory of Molecular Biology
Francis Crick Avenue
Cambridge CB2 0QH
UK

1: These authors contributed equally

*: Corresponding authors: sean@mrc-lmb.cam.ac.uk and ag@mrc-lmb.cam.ac.uk

Abstract

The GTPases of the Ras superfamily regulate cell growth, membrane traffic and the cytoskeleton, and a wide range of diseases are caused by mutations in particular members. They function as switchable landmarks with the active GTP-bound form recruiting to the membrane a specific set of effector proteins. The GTPases are precisely controlled by regulators that promote acquisition of GTP (GEFs) or its hydrolysis to GDP (GAPs). We report here MitoID, a method for identifying effectors and regulators by performing in vivo proximity biotinylation with mitochondrially-localized forms of the GTPases. Applying this to 11 human Rab GTPases identified many known effectors and GAPs, as well as putative novel effectors, with examples of the latter validated for Rab2, Rab5 and Rab9. MitoID can also efficiently identify effectors and GAPs of Rho and Ras family GTPases such as Cdc42, RhoA, Rheb, and N-Ras, and can identify GEFs by use of GDP-bound forms.

Introduction

The timing and location of many cellular events is controlled by small GTPases of the Ras superfamily (Takai et al., 2001). These proteins share a similar nucleotide-binding fold, with the arrangement of surface loops altered depending on whether GTP or GDP is bound (Vetter and Wittinghofer, 2001). Although often called GTPases, they typically lack intrinsic GTPase activity and instead nucleotide status is determined by regulatory proteins that either stimulate GTP hydrolysis, or exchange GDP for GTP (Müller and Goody, 2018; Barr and Lambright, 2010; Cherfils and Zeghouf, 2013). This allows the G protein's binding interactions to be regulated and hence they act as molecular switches that generally only bind their effectors when in the GTP-bound state. In this way upstream regulators can control precisely the location or activity of numerous cytosolic proteins.

The Ras superfamily can be divided into five major families based on sequence and function: the Rab and Arf families that regulate membrane traffic, the Rho family that regulates cytoskeletal dynamics, the Ras family that regulates cell proliferation and differentiation, and Ran that directs nuclear transport (Rojas et al., 2012; Colicelli, 2004). The large majority of the Ras superfamily GTPases are lipid modified to allow transient attachment to membranes in the active state. The Ras, Rab and Rho families have prenyl groups attached to one or more cysteines at their C-termini, whilst Arfs have a myristoyl group on the N-terminus and Ran is not lipidated. The biological importance of these families is reflected by the fact that their mutation underlies major human diseases. Mutations in the various types of Ras are present in many cancers, and mutations in other members of the superfamily cause disorders of the immune system, the nervous system or of development (Hutagalung and Novick, 2011; Hobbs et al., 2016; Maldonado and Dharmawardhane, 2018).

Understanding the biology of small GTPases requires identifying their upstream regulators and their downstream effectors. Although a lot of progress has been made with some GTPases, the superfamily comprises 167 members in humans and many remain less well understood (Rojas et al., 2012; Colicelli, 2004). In

addition, new effectors and regulators continue to be identified for even the well-studied members of the family, and it is likely that the repertoire of interactors will vary between different cell types. The two main approaches that have been used for finding effectors have been yeast two-hybrid screens and affinity chromatography (Gillingham et al., 2014; Fukuda et al., 2008; Christoforidis et al., 1999a). Both take advantage of mutations that in many members of the family lock the G protein in an active or inactive conformation (Vetter and Wittinghofer, 2001; Itzen and Goody, 2011; Feig, 1999; Der et al., 1986). Although both approaches have had successes they also have limitations. The yeast two-hybrid method relies on both GTPase and effector folding correctly in yeast, and because only a single gene is tested at a time, it precludes detection of effectors that are protein complexes, or at least require associated proteins for stability. The affinity chromatography approach can detect binding to protein complexes, but requires production of correctly folded GTPase, and typically requires large amounts of cell lysate, and interactors have to bind tightly enough to persist during the column washing that is required to remove the rest of the cell lysate before the interactors are eluted and identified.

Recently, proximity biotinylation has emerged as a new approach for identifying protein-protein interactions. If a protein of interest is expressed in cells as a fusion to a promiscuous biotin ligase (BioID) or an engineered peroxidase (APEX) then proteins in the vicinity become biotinylated and can be isolated with streptavidin and identified by mass-spectrometry (Roux et al., 2012; Martell et al., 2012). However, applying this to small GTPases is potentially problematic since the fusion to the protein that generates biotin must not interfere with effector binding or membrane targeting. In addition, in order to distinguish specific interactors from those biotinylated because they simply happen to be in the same location it is important to compare several different fusion proteins that have a similar location, and yet different GTPases typically act on different membranes making direct comparison more challenging. In addition the GDP-bound forms that are used as a control in yeast two-hybrid and affinity chromatography are generally not membrane bound and so will have a different background set of bystanders to the GTP-bound

form. Here we report a BioID-based approach in which we compare many different small GTPases relocated to the same location - the mitochondrial outer membrane. We find that in this ectopic location there is a similar set of background interactions, but each G protein also interacts with specific effectors and regulators which can be readily identified by comparative analysis.

Results

Relocation of Ras family GTPases to mitochondria.

To perform BioID with Ras family GTPases we established a system to express them as fusions to the BirA* promiscuous biotin ligase whilst ensuring that they are all at a standard location so as to allow direct comparison (Figure 1A). Mitochondria have proven useful for ectopic relocation of cytosolic proteins as there are well defined targeting signals for inserting proteins into the outer membrane of mitochondria without interfering with mitochondrial function (Silvius et al., 2006; Mitoma and Ito, 1992; Hoogenraad et al., 2003). Moreover, proteins directed to mitochondria will have a tightly restricted distribution. Mitochondria have a relatively large area of membrane in which to accommodate an exogenous protein, and by using a mitochondrial transmembrane domain there is little risk of exchange into the cytoplasm. To test this approach we expressed in cells a form of the endosomal Rab protein Rab5A in which the two C-terminal cysteines that receive lipid modification were replaced with the mitochondrial targeting sequence of monoamine oxidase (Figure 1A). The BirA* biotin ligase was placed after the C-terminal unstructured linker of the GTPase but before the mitochondrial transmembrane domain, a position close enough to the switch regions to modify effectors without interfering with their binding. Rab5A was expressed with single residue changes that are known to lock it into either the GTP-bound form by blocking GAP activity (Q79L) or the GDP-bound form by interfering with GTP binding (S34N) (Li and Stahl, 1993; Stenmark et al., 1994).

When expressed in cells the Rab5A chimeras were located on mitochondria, and probing with streptavidin revealed accumulation of biotin on mitochondria indicating that the BirA* part of the chimera had retained activity (Figure 1B,C). The presence of Rab5A on mitochondria did not result in the wholesale relocation of endosomes to the mitochondrial surface, and hence biotinylation of endosomal proteins should reflect interaction with Rab5 and not altered location of the organelle (Figure 1D). We also tested a Rab from a different location, the Golgi-

localized Rab, Rab2A, and again found mitochondrlal accumulation of the chimera, but no gross relocation of the Golgi itself (Figure 1E,F).

Biotinylation of proteins by mitochondrial Rab5A-BirA* chimeras.

To determine if the Rab5A-BirA* chimeras biotinylated known interacting proteins, biotinylated proteins were isolated from cells expressing the GTP-bound or GDP-bound forms, and identified by mass-spectrometry. The experiment was performed in triplicate, and to visualise the outcome the mean of the total spectral counts obtained for each protein with the GTP-bound form (Rab5A(Q79L)) was plotted against the same for the GDP-bound form (Rab5A(S34N)). As expected, the highest counts were obtained from Rab5A itself and endogenous enzymes that contain a biotin prosthetic group, and these, along with abundant cytosolic proteins, were found with both Rab5A forms (Figure 2A). Examining the proteins with lower counts revealed that ~20 proteins known to bind directly to Rab5-GTP, or to be subunits of complexes that bind to Rab5-GTP, where found to be biotinylated specifically by the GTP-bound form (Figure 2B). These include canonical Rab5 effectors such as EEA1, Huntingtin and Rabenosyn-5; as well as subunits of complexes that bind Rab5 such as CORVET, class III PI 3-kinase, and FTS/Hook/p107^{FHIP} (Wandinger-Ness and Zerial, 2014; Xu et al., 2008; Simonsen et al., 1998; Nielsen et al., 2000; Christoforidis et al., 1999b).

We also looked at known regulators of Rab5A. Strikingly, three Rab5 GEFs appeared in the dataset, of which GAPVD1/Rme-6 and ALS2/alsin were predominantly present with the GDP-bound form (Figure 2B). The third GEF, Rabex-5, was found at similar levels with both Rab5A mutants, but it is known to form a complex with Rabaptin-5, an effector for Rab5A, an interaction thought to amplify Rab5 activation (Horiuchi et al., 1997).

Almost all of these known Rab5 effectors and GEFs were detected in all three of the biological replicates used to calculate the mean values, indicating that the approach is robust and reproducible (Figure 2C). Taken together, these results indicate that when Rab5A is fused to BirA* and relocated to the surface of

mitochondria it is still able to bind effectors and regulatory proteins in a nucleotide-specific manner. More importantly, these interactions are stable enough for the interaction partners to become biotinylated by BirA* and hence identified by BioID.

Application of MitoID to a wide range of Ras family GTPases

The above results with Rab5A are a promising indication that the MitoID approach is an effective general means of identifying the binding partners of small GTPases. However Rab5 is one of the most abundant small GTPases in cultured cells, suggesting that its interactors may also be relatively abundant. Indeed it is one of the few mammalian Rabs for which there is a report of a large scale identification of effectors by affinity chromatography (Christoforidis et al., 1999a). To determine if the MitoID approach is broadly effective for small GTPases we applied it to a panel of sixteen other small GTPases. These include ten further Rab GTPases: Rab2A, Rab6A, Rab18, Rab30 and Rab33B from the Golgi, Rab8A and Rab10 from post-Golgi carriers, Rab11A from recycling endosomes and Rab7A and Rab9A from late endosomes (Hutagalung and Novick, 2011). In addition we examined Cdc42, Rac1 and RhoA from the Rho family and Rheb, RalA and N-Ras from the Ras family. All sixteen GTPases were expressed in HEK293 cells as fusions to mitochondrial BirA* with residue changes known, or predicted, to lock them in the GTP-bound or GDP-bound states (Der et al., 1986; Feig, 1999). Immunofluorescence showed that all of the chimeras accumulated on mitochondria (see Figure 1-figure supplement 1A,B for representative examples). Biotinylation and streptavidin purification was performed as before with three biological replicates for each chimera.

Analysis of protein-protein interaction data from conventional coprecipitation experiments has shown that comparing the results from one bait to those from many other baits increases the sensitivity and accuracy with which true interaction partners can be identified (Huttlin et al., 2015; Hein et al., 2015). Several methods have been developed for such analysis based on either spectral counts or spectral intensities, and we analyzed our data with one of each. The CompPASS platform uses spectral counts and assigns to each hit a “D-score” based on the counts but

weighted up for the number of times it is replicated with a given bait, and weighted down in proportion to the number of other baits which give the same hit (Sowa et al., 2009). The Perseus platform uses spectral intensity and compares the replicates of one bait to those for all other baits to calculate a fold enrichment for the hits and a statistical confidence for that enrichment, with the two being plotted against each other to generate a 'volcano' plot (Keilhauer et al., 2015). For both methods consideration has to be given to the likelihood that a real hit with one bait could also be a bona fide interaction partner with other baits used as controls as this could reduce the significance assigned. Given that some effectors are known to be shared by several Rabs or several Rhos then this is likely to be the case here. Thus for the D-score we used the WD variant that gives extra weight to interactions where several baits show significantly higher spectral counts than the mean for the whole dataset (Behrends et al., 2010). For the volcano plots based on spectral intensity we compared the GTP-bound form to the complete set of GDP-bound forms on the grounds that effectors generally do not bind the GDP-form. The GDP-forms were also compared to all other GDP-bound forms as it is unlikely that exchange factors act on more than one or two specific GTPases.

Application of MitoID to the GTP-bound form of Rab5A

When the WD score method based on spectral counts was applied to GTP-bound Rab5A it worked well to enrich known Rab5 effectors with there being eighteen known effectors in the top twenty hits (Figure 3A,B). Likewise, in a volcano plot based on spectral intensities many known Rab5 effectors were amongst those whose enrichment over background has the highest statistical significance (Figure 3C). It is possible to combine the two scorings systems in a bubble volcano plot, with the area of the data point being proportional to the WD score (Figure 3D). The hits with high WD scores are all amongst the most significant hits in the volcano plot indicating a good correlation between the two methods.

In addition to known effectors, there were a number of high scoring hits that have not previously been linked to Rab5. Interestingly, several of these have been

reported to act in the endocytic system such as the lipid phosphatase INPP4A (Nigorikawa et al., 2015), the PX-domain containing kinase RPS6KC1 (Liu et al., 2005), the TSC1 and TSC2 subunits of the Rheb GAP (Manning and Cantley, 2003), and the V-ATPase regulator WDR7/Rabconnectin-3β (Sethi et al., 2010). Other hits include OSBPL9 and its paralog OSBPL11, and the protein RELCH. RELCH was also a hit with Rab11A (Figure 3B), and has recently been reported to be Rab11A effector and to have a role in lipid transport (Sobajima et al., 2018). To determine if our approach had correctly identified novel Rab5 effectors, OSBPL9 and KIAA1468/RELCH were selected for validation as described below.

These findings show that both methods of analysis correctly identify known Rab5A effectors as the highest hits. The WD-score plot allows an overview of interactions with other GTPases but the bubble-volcano plots are a much more compact means of presenting the hits with a particular Rab. Thus we summarise below the findings with each GTPase using bubble-volcano plots, with the spectral counts, WD scores and peak intensities for all GTPases provided in Supplementary files 1 and 2, and the data used for the plots in Supplementary files 3 and 4. The summaries of the results with Rab GTPases is followed by experimental validation of selected novel hits and the summaries of the results with the Ras and Rho family GTPases.

Application of MitoID to a panel of Rab GTPases

In addition to Rab5A, we tested ten other members of the Rab family (Figures 4-6). We first summarise the findings with the GTP-bound forms, followed by those cases where the GDP-bound form was informative.

Rab2A: Rab2 is conserved in many eukaryotic phyla and appears to have a dual role on both the Golgi and the endocytic pathway. With Rab2A-GTP the twelve highest scoring hits include four proteins known to bind Rab2 or be in complexes reported to bind Rab2 (Figure 4A). These include the coiled-coil protein CCDC186/CCCP-1, a subunit of the COG vesicle tethering complex, and the

Bicaudal dynein adaptor (Gillingham et al., 2014; Ailion et al., 2014). A further seven proteins in the top twelve have been implicated in membrane traffic (e.g. GBF1, RUFY1, WDR11), or are proteins of unknown function that are related to known components of membrane traffic (ARFGEF3).

The next 30 hits include 16 proteins with links to membrane traffic of which six are known Rab2 interactors. The interactors include both subunits of the PICK1:ICA1 complex that acts in secretory granule biogenesis, BLZF1/golgin45, USO1/p115 and INPP5B; as well as TBC1D25/OATL1 that has been reported to be a Rab2 GAP (Itoh et al., 2006; Buffa et al., 2008; Short et al., 2001; Williams et al., 2007). Of the hits not associated with membrane traffic most are involved with centrosomes and cilia. These may be spurious interactions, but there is evidence that the Golgi is associated with centrioles and with ciliogenesis (Hua and Ferland, 2018; Barker et al., 2016). The remainder are two proteins of unknown function (STAMBPL1 and FAM184A) and an abundant cytosolic enzyme argininosuccinate synthetase which seems unlikely to be valid. Thus MitoID identified known effectors of Rab2, and several putative novel effectors, of which ARFGEF3 and STAMBPL1 were selected for validation as described below.

Rab6A: Rab6 is conserved in most, if not all, eukaryotes and acts on the trans Golgi network, particularly in recycling from endosomes (Pfeffer, 2011). Almost half of the top thirty hits with Rab6A-GTP are known Rab6 effectors, including p150/glued subunit of dynactin (DCNT1), the Rab39 GEFs DENDD5A and DENND5B, the dynein adaptor bicaudal-1/2, the Rho GEF ARHGEF1 and the coiled-coil proteins ERC1/2 and TMF1 (Short et al., 2002; Matanis et al., 2002; Fukuda et al., 2011; Shibata et al., 2016; Fridmann-Sirkis et al., 2004) (Grigoriev et al., 2007) (Figure 4B). In addition, RABGAP1 and its paralog RABGAP1L have been reported to have GAP activity on Rab6 (Cuif et al., 1999). There are also several proteins previously linked to membrane traffic at the Golgi and endosomes that are not known Rab6 effectors including the lipid phosphatases MTMR1 and INPP5F, the Beach domain protein

WDFY3, the microtubule regulator PDE4DIP/myomegalin, and kinesin light chain; as well as MB21D2, a protein of unknown function.

Rab7A: Rab7 is conserved in most eukaryotes and acts on late endosomes to control their maturation and fusion with lysosomes. The top hits with Rab7A-GTP include three known effectors: Epg5, Vps13C and WDR91; a known Rab7 GAP, TBC1D5; and the Rab geranyltransferase subunit CHML (Wang et al., 2016; Tabata et al., 2010; Casanova and Winckler, 2017; Seaman et al., 2009) (Figure 4C). Other strong hits include the PtdIns 5-kinase PIKFYVE which is found on Rab7-containing late endosomes, and WDR7 and DMXL1, which are orthologs of the subunits of the rabconnectin dimer that controls V-ATPase activity in the endosomal system (Sbrissa et al., 2002; Sethi et al., 2010; Yan et al., 2009). UHFR1BP1 has no reported function, but is a paralog of UHFR1BP1L/SHIP164 which was reported to be localized to endosomes and to interact with SNARE proteins (Otto et al., 2010).

Rab9A: Rab9A is a relative of Rab7 that emerged early in metazoan evolution and also acts on endosomes. The top WD scores with the GTP form of Rab9A include several proteins known to act on endosomes including the scaffold protein GRIPAP1/GRASP-1; the HPS3 subunit of the BLOC-2 complex that regulates endosomal traffic; the sorting nexin Snx13 and its paralog Snx14; and the monooxygenase MICALL1 (Gautam et al., 2004; Zheng et al., 2006; Beer et al., 2018; Hoogenraad et al., 2010; Sharma et al., 2009) (Figure 4D). Other hits included the known Rab9 effector GCC2/golgin-185 and the dynein regulator NDE1/NudE, which was reported as a hit with Rab9 in a yeast two-hybrid screen but did not show nucleotide-specific binding by co-precipitation with Rab9B (Bradshaw and Hayashi, 2017). Of these hits we selected HPS3 and NDE1 for validation as described later.

Rab8A and Rab10: Rab8 and Rab10 arose from a gene duplication early in metazoan evolution and have related roles in exocytosis including sharing some

effectors (Sato et al., 2014; Elias et al., 2012; Kloepper et al., 2012). The high scoring hits with the GTP-bound form of Rab8A include known effectors such as synaptotagmin-like 4 (SYTL4), the myosin MYO5A, the lipid phosphatase OCRL, the Rho GEF ARHGEF10, and the flavoprotein monooxygenases MICALL1 and MICAL3, with the latter four also being hits for Rab10 (Fukuda et al., 2002; Shibata et al., 2016; Sharma et al., 2009; Grigoriev et al., 2011; Sun et al., 2014) (Figure 4E,F). The Ste20 kinase MAP4K3 and its paralog MAP4K5 were hits with both Rab8A and Rab10. MAP4K3 has recently been reported to co-precipitate with Rab8A, and another paralog, MAP4K2, was reported to bind Rab8 (Steger et al., 2017; Ren et al., 1996). The other top hits with Rab10 include the known effectors MYO5C and several subunits of the exocyst complex including its direct binding partner EXOC6 (Sano et al., 2015; Roland et al., 2009). Other strong hits include the motor proteins MYO18A and kinesin-2 KIF3A/B.

Rab11A: Rab11 is conserved in most eukaryotes and participates in traffic through recycling endosomes and the trans Golgi network (Wandinger-Ness and Zerial, 2014). Amongst the top ~30 hits are thirteen known Rab11 effectors: the Rab8 GEF Rab3IP/Rabin8, the Rab GAP TBC1D12, the PI 4-kinase PI4KIIIβ, subunits of the exocyst complex, the A-kinase-anchoring protein D-AKAP2/AKAP10, the kinesins KIF13A/B, and the proteins of unknown function WDR44/Rab11BP and RELCH/KIAA1468 (Knödler et al., 2010; Sobajima et al., 2018; Longatti et al., 2012; Zeng et al., 1999; Eggers et al., 2009; Oguchi et al., 2017; Etoh and Fukuda, 2019) (Figure 5A). In addition, the hits include two TBC domain GAPs reported to act on Rab11, EVI5 and RABGAP1 (Fuchs et al., 2007; Laflamme et al., 2012). Interestingly most of the remaining hits are proteins linked to endosome function but not reported as Rab11 effectors, including the coiled-coil protein RUFY1, the Vps8 subunit of the CORVET complex, and UHRF1BP1L.

Rab18: Rab18 is conserved in many phyla but its role remains to be fully resolved with evidence for action in both ER to Golgi traffic and in lipid droplet function

(Gerondopoulos et al., 2014; Dejgaard et al., 2008). The top hits with the GTP-bound form included the NAG/NBAS and Zw10 subunits of the ER-associated NAG-RINT1-ZW10 (NRZ) tethering complex, and the Rab7 GAP TBC1D5, with both of these having been previously reported as Rab18 interactors (Xu et al., 2018; Gillingham et al., 2014) (Figure 5B). The other top hits were SCFD2, a poorly characterized relative of the Sec1 SNARE binding protein that has been reported to interact with subunits of the NRZ complex (Tagaya et al., 2014; Huttlin et al., 2015), and the Bicaudal dynein adaptor which is known to interact with several other Rabs.

Rab30: Rab30 is a relative of Rab1 that emerged early in metazoan evolution, and is localized to the Golgi although its role is unclear (Kelly et al., 2012). Hits with Rab30 included subunits of the GARP complexes which were also found by affinity chromatography to bind to *Drosophila* Rab30, and PHLDB3, a protein of unknown function found to co-precipitate with Rab30 in a large scale proteomic screen (Huttlin et al., 2017; Gillingham et al., 2014) (Figure 5C).

Rab33B: Another relative of Rab1, Rab33 also emerged early in metazoan evolution with two paralogs arising with the expansion of vertebrates, both of which contribute to membrane traffic at the Golgi apparatus (Zheng et al., 1998). High scoring hits included three previously reported effectors: RUFY3, the RABEP1/RABGEF1 (Rabex5/Rabaptin) complex, and the golgin GCC2/golgin-185 (Valsdottir et al., 2001; Fukuda et al., 2011; Hayes et al., 2009) (Figure 5D). Other hits include several centrosomal protein, the plausibility of which remains unclear, and members of the MICAL family which bind Rab1 and several other Rabs (Rai et al., 2016).

GDP-locked forms of some Rabs can detect exchange factors.

Most, if not all, Rabs are activated by GEFs that open the nucleotide-binding pocket and thus release bound GDP and enable binding of GTP. In those cases characterized, the GEF binds more tightly to the nucleotide-free form than the GTP-bound form to allow release of the latter following exchange (Müller and Goody,

2018; Cherfils and Zeghouf, 2013) (Langemeyer et al., 2014; Koch et al., 2016; Feig, 1999). Thus mutations which interfere with GTP-binding stabilize the interaction with the GEF, and overexpression can cause a dominant negative suppression of activation of the endogenous Rab. In this study we have used the canonical GDP-locked forms in which the conserved P-loop serine or threonine is replaced with asparagine. This mutation has been shown to prevent GTP binding, but it also reduces affinity for GDP, and hence it is regarded as a hybrid GDP-bound and nucleotide-free form (Koch et al., 2016; John et al., 1993). In contrast to our findings with the GTP-locked forms, most of the S/T->N forms of the Rabs do not show any highly significant interactions (illustrated for Rab6A(T27N) in Figure 6A). However, three Rabs showed strong and reproducible interactions with known or putative exchange factors.

Rab2A(S20N) gave two strong hits (Figure 6B). The first is Clec16A, a protein linked to autophagy, with the *C. elegans* ortholog, GOP-1, reported to be required for Rab2 activation in vivo and in vitro (Yin et al., 2017; Redmann et al., 2016). The second strong hit is TBC1D25/OATL1 which, as noted above, has been reported to be a Rab2 GAP, suggesting that it can bind both forms of the GTPase prior to GTPase stimulation. With Rab5A(S34N) the five most significant hits include the Rab5 GEFs alsin/Als2 and GAPVD1/Rme-6, and the subunits of the dimer formed by the Rab5 GEF rabex5/RABGEF1 and rabaptin-5/RABEP1 (Figure 6C). The remaining protein, FAM135A, has no previously reported function. Finally, with Rab11A(S25N) the two top hits were the C9 and C10 subunits of the TRAPPII complex that activates Rab11 (Riedel et al., 2017) (Figure 6D). The other two known Rab11 GEFs, SH3BP5 and its paralog SH3BP5L were also hits, along with PI 4-kinase that binds Rab11 in a nucleotide-independent manner and the Rab geranyltransferase subunit CHML (Sakaguchi et al., 2015; Burke et al., 2014). Taken together, these results show that MitoID can also detect interactions between the GDP-bound/nucleotide free versions of Rabs and their exchange factors.

Validation of novel interaction partners for Rab2A, Rab5A, and Rab9A.

The GTP-forms of the eleven Rabs analysed here all had highly significant hits that have not previously been reported to be GTPase effectors. To further validate the MitoID approach we tested a subset of these hits.

The highly significant hits for Rab2A-GTP included STAMBPL1 and ARFGEF3. STAMBPL1 is a paralog of STAMBP (AMSH), an endosome-associated deubiquitinase that regulates entry of endocytosed proteins into the ESCRT-dependent multi-vesicular body pathway (Clague and Urbé, 2006). Although STAMBPL1 has been shown to share with STAMBP a specificity for cleaving Lys63-linked polyubiquitin chains, its function is unclear (Sato et al., 2008). ARFGEF3 (BIG3) is a member of the Sec7 domain family of Arf GEFs, and regulates insulin granule formation via an unknown mechanism (Li et al., 2014). Both STAMBPL1 and ARFGEF3 specifically bound to Rab2A-GTP when cell extracts were applied to GST-Rab-coated beads (Figure 7A). In addition, GFP-tagged forms of the proteins showed a striking relocation to mitochondria when co-expressed with the mitochondrial form of Rab2A-GTP (Figure 7B,C). Finally we were able to express recombinant STAMBPL1 and this bound directly to recombinant Rab2A (Figure 7D). These findings clearly suggest that Rab2 can recruit STAMBPL1 and ARFGEF3 to membranes, and imply that both proteins are regulated, at least in part, by Rab2. Interestingly there is evidence that ARFGEF3, like Rab2, has a role in secretory granule biogenesis (Buffa et al., 2008; Csizmadia et al., 2018; Sumakovic et al., 2009).

Rab5A-GTP gave several novel hits including OSBPL9, RELCH and TBCK. OSBPL9 (ORP9) is a member of a family of cholesterol transfer proteins that binds to the protein VAP in the ER and to PtdIns(4)P on the Golgi and endosomes (Ngo and Ridgway, 2009; Dong et al., 2016). RELCH has recently been reported as a Rab11 effector and to have a role in cholesterol transport (Sobajima et al., 2018). TBCK has a kinase domain and a TBC domain that is found in many Rab GAPs, but its function is unknown (Chong et al., 2016). All three proteins bound specifically to the GTP form of Rab5 when cell extracts were passed over Rab5-coated beads

(Figure 7E). In addition, a GFP-tagged form of TBCK relocalized to mitochondria when co-overexpressed with mitochondrial Rab5-GTP (Figure 7F).

Rab9 is located on late endosomes and has many fewer reported effectors than Rab2 or Rab5, and so it was interesting to find several strong novel hits. We selected for analysis NDE1, a dynein regulator, and the HPS3 subunit of the BLOC-2 complex that has an unresolved role in the biogenesis of lysosome-related organelles (Dennis et al., 2015; Bradshaw and Hayashi, 2017). For NDE1 it was possible to express the protein in E. coli, and this recombinant protein bound directly to the GTP-from of Rab9A (Figure 7G). There were no suitable antibodies to investigate HPS3, but when epitope-tagged HPS3 was co-expressed in cells with mitochondrial Rab9A it was efficiently recruited by the GTP form but not the GDP form, and the same tagged proteins showed GTP-specific binding to a Rab9A affinity column (Figure 7H,I). Rab9 recruiting to endosomes NDE1 and the BLOC-2 complex would be consistent with NDE1 being required for endosomal positioning and Rab9 having a role in melanosome biogenesis (Mahanty et al., 2016; Lam et al., 2010). Taken together these results show that the MitoID method is capable of identifying novel effectors of even well studied Rabs.

Application of MitoID to Ras GTPases

The Rabs are only one of five families within the Ras superfamily of Ras GTPases (Rojas et al., 2012; Takai et al., 2001; Colicelli, 2004). To determine if the MitoID approach was broadly applicable we tested it with representative GTPases from the Rho and Ras families. The Ras GTPases have diverse roles in regulation of cell growth and differentiation (Hobbs et al., 2016; Heard et al., 2014; Gentry et al., 2014). To assess the applicability of MitoID to this family we selected three well characterized members: N-Ras, RalB and Rheb.

N-Ras: One of several closely related Ras GTPases that act in signaling pathways controlling cell growth and that have received extensive attention due their being oncogenes (Hobbs et al., 2016). With the GTP-bound form of N-Ras, the top five hits

comprise two Ras effectors (the kinases RAF1/c-Raf and BRAF1/B-Raf), the Ras GAP NF1/neurofibromin-1, and the closely related proteins RAPGEF2 and RAPGEF6 (Figure 8A). The latter two proteins act on Rap1, but also have a Ras associating (RA) domain found in other proteins to bind Ras or other small GTPases. RAPGEF2 has been reported to bind Rap1 but there is no report of an interaction with N-Ras (Rebhun et al., 2000; Liao et al., 1999). With the GDP-form of N-Ras the top hit is the Ras GEF SOS1 (Figure 8B), with there also being an interaction with RAP1GDS1 that has a chaperone-like role and binds Ras irrespective of its nucleotide state (Vikis et al., 2002).

RalB: The Ral GTPases regulate various events at the cell surface including exocytosis and cell migration (Gentry et al., 2014). The top ten most significant hits with the GTP form of RalB include six subunits of the exocyst vesicle tethering complex, a known RalB effector, including the EXOC2/Sec5 subunit to which RalB binds directly (Sugihara et al., 2002) (Figure 8C). The hits also include the Ral effector RLIP/RalBP1 and its binding partner REPS1/Reps1, and the subunits of the two known Ral GAPs (RALGAPA1/2 and RALGAPB) (Yamaguchi et al., 1997; Shirakawa et al., 2009). The other more significant hits are nucleic acid binding proteins that seem likely to be contaminants. The GDP-bound form of RalB did not give a significant score with any known or plausible GEF.

Rheb: The small GTPase Rheb is a major regulator of the mTORC1 kinase complex that controls protein synthesis and cell growth (Heard et al., 2014). The top hit with the GTP-bound form of Rheb is the mTORC1 subunit Raptor that is located next to the Rheb binding site on mTor (Yang et al., 2017) (Figure 8D). The next two hits are Tsc1 and Tsc2, the subunits of the Rheb GAP that controls the activity of Rheb and hence mTORC1 (Manning and Cantley, 2003). The remaining hits have substantially lower scores. The mechanism by which Rheb is activated is not known, and the hits with the GDP-bound form seem unlikely to be meaningful as they have known functions unrelated to growth control.

Application of MitoID to Rho GTPases

The Rho family is another of the five sub-families that comprise the Ras superfamily. The Rho GTPases are major regulators of the actin cytoskeleton (Heasman and Ridley, 2008; Narumiya and Thumkeo, 2018), and we tested the MitoID approach with three of the best characterized members of the family: Cdc42, RhoA, and Rac1. As with the other GTPase we used mutant forms predicted to be locked in the GTP-bound or GDP-bound states, and the findings are summarised below.

Cdc42: The top 25 most significant hits with the GTP-form of Cdc42 include 19 known Cdc42 effectors (including kinases, actin regulators and scaffolding proteins), two known Cdc42 GAPs (ARHGAP31/32), and myosin18A that has been reported to form a complex with CDC42BPB, one of the Cdc42 effectors (Tan et al., 2008; Vigil et al., 2010) (Figure 9A). The remaining proteins include KCTD3, a putative linker to cullin E3 ligase (Pinkas et al., 2017). Its function is unknown, but its paralog SHKBP1 is also present in the list of hits. In addition some hits are regulators of other members of the Rho family such as the RhoA GEFs ARHGEF11/PDX-RhoGEF, ARHGEF12/LARG, ARHGEF40/Solo and PLEKHG4 reflecting the known cross talk between the Rho family GTPases (Paul et al., 2017).

With the GDP-locked form of Cdc42 the top hits include four members of the DOCK family of Rho GEFs that are known to activate Cdc42, along with LRCH2 and LRCH3 that have recently been found to interact with a subset of DOCK family GEFs (O'Loughlin et al., 2018) (Figure 9B). The other hits include ARHGAP32/p250GAP, a Rho family GAP reported to act on Cdc42 and RhoA (Nakazawa et al., 2003). ARHGAP32 was found with both GDP and GTP forms of Cdc42 suggesting its substrate recognition is not sensitive to nucleotide state. Interestingly, one of the lower significance hits was PDLIM4, a member of the ‘enigma’ family of LIM/PDZ domain proteins. These proteins interact with the actin cytoskeleton, with one recently reported to be required for activation of Cdc42 (Velthuis and Bagowski, 2007; Liu et al., 2015).

RhoA: The top 35 hits with GTP-locked RhoA include 19 known effectors including kinases like PKN1 and CIT/Citron, scaffolds like the Rhotekins RTKN/RTKN2, RhoA GEFs such as ARHGEF1/p115-RhoAGEF and ARHGEF12, and phosphatases such as INPPL1/SHIP (Figure 9C). In addition there are six known RhoA GAPs such as ABR, ARHGAP5, ARHGAP35/p190RhoGAP. The remaining strong hits include the dynein adaptor BICD, a sorting nexin, and four DNA or RNA binding proteins (GEMIN4/5, GCFC2 and MCM4) which seem likely to be contaminants. With the GDP-locked form of RhoA the top four hits are all known RhoA GEFs, with further other GEFs with lesser scores (Figure 9D). The top four were also hits mentioned above with the GTP-form of RhoA reflecting the fact that they are also effectors that act in a positive feedback loop (Medina et al., 2013).

Rac1: Initial application of MitoID to Rac1 revealed known interactors but also showed Rac1-specific biotinylation of many DNA or RNA binding proteins, with these interactions typically being nucleotide-state independent (Figure 9-figure supplement 1A). Some Ras family GTPases have poly-basic stretches next to their C-terminal lipid anchors which stabilize interactions with acidic phospholipids in the cytosolic leaflet of the plasma membrane. On the neutral membranes of mitochondria these basic residues might instead recruit nucleic acids and so we repeated the MitoID with Rac1 lacking the six consecutive basic residues adjacent to the lipid anchor. This reduced the number of nucleic-acid binding proteins but did not prevent interactions with effectors and so our analysis was performed with this version of Rac1 (Figure 9-figure supplement 1B).

The top eight hits with Rac1-GTP are all known Rac1 effectors, the GIT/PIX (ARFGEF6/7) complexes that are also Cdc42/Rac1 GEFs, the PAK2 kinase and the WASF2, ABI1 and CYFIP subunits of the WAVE2 actin regulatory complex (Figure 9E). The next 30 most significant hits include ten further Rac1 effectors, and six Rac1 GAPs. The remaining proteins include several uncharacterized members of the ARHGEF and ARHGAP families of Rho GTPase regulators, and NHSL1, one of three

paralogs of the Nance-Horan syndrome protein. The function of the NHS family of proteins is unknown, but interestingly they have a WAVE homology domain and their knockdown perturbs the actin cytoskeleton (Brooks et al., 2010).

With the GDP-locked form of Rac1 the top four hits are members of the DOCK family of Rho GEFs (Figure 9F). Interestingly, DOCK6 and DOCK7 were found with both Rac1 and Cdc42 whereas DOCKs 1,4 and 5 were specific to Rac1 and DOCKs 9 and 11 were specific to Cdc42, accurately reflecting their known substrate specificity (Gadea and Blangy, 2014).

Taken together these results provide overwhelming evidence that the MitoID approach works not only with Rab GTPases but also with the members of the Ras and Rho families of GTPases.

Discussion

Proximity biotinylation has emerged as a powerful method for identifying the interaction partners of proteins (Lambert et al., 2015; Roux et al., 2012). However, like other methods aimed at this goal it generates not just signal but also noise, which in this case comes from bystander proteins that are not direct interactors. Again, as for other methods, specific interactions can be identified by comparing many baits, but this requires the noise to be as uniform as possible. We show here that relocating a set of baits to the same ectopic location can still be compatible with binding to known interactors whilst allowing the advantage of meaningful comparison between baits.

The method has several further advantages over more conventional approaches based on affinity chromatography or yeast two-hybrid screening. Expressing human proteins in cultured cells allows access to relevant chaperones or post-translational modifications, maximising the chance that the bait is active. The binding is assayed in living cytosol and hence at native protein and ion concentrations. As the protein is at an ectopic location with a large capacity to handle exogenous proteins then over-expression should increase the biotinylation of targets without the risk of accumulation in an undesired location. Finally, it should be noted that the method does not require a very large number of cells. For each replicate we used two T175 flasks totalling 5×10^7 cells that were transiently transfected with the expression plasmid, and so MitoID should be readily applicable to comparing different cell types.

However, it is also important to acknowledge the method has some limitations. Firstly, it is possible that some GTPase effectors will require a specific lipid for stable membrane association, although we were able to find binding partners for GTPases from several different locations that are known to differ in lipid composition. Secondly we only found known GEFs with a subset of the Rab GTPases. This may reflect that fact that the canonical “GDP-locked” mutation used in this study has a complex effect in that it destabilises the binding of both GTP and GDP but the latter interaction is less affected in the limited number of cases

examined (Koch et al., 2016; John et al., 1993). Although all Ras superfamily members share the same general fold it is known that the precise details of their structure and activation cycle are somewhat variable (Langemeyer et al., 2014; Merithew et al., 2001; Cherfils and Zeghouf, 2013; Eathiraj et al., 2005). In this context it has been reported that the “GDP-locked” form of Rab27A is rapidly degraded in vivo suggesting the mutation destabilises the protein (Ramalho et al., 2002). Thus it may be that successful application of MitoID with the GDP-locked form requires that the empty state is not only stable but also able to bind the GEF sufficiently tightly to allow detection. Thirdly, although we found known effectors with all of the non-Rab GTPases examined, we did not find high confidence hits with a few Rabs that we tested including Rab7L1, Rab19, and Rab39 and so they were not included in the analysis. These Rabs are known to be much less abundant than the Rabs presented here and so it is possible that their effectors are too scarce to be detected with the conditions used (Hein et al., 2015).

Despite these caveats, the MitoID approach has clear potential for analysing the roles of the many less well characterized members of the Ras superfamily. In addition, there is scope for addressing the few limitations of the method. Our approach relied on using the original BirA* biotin ligase but more active variants have been recently reported (Branon et al., 2018; Kim et al., 2016). Likewise, the sensitivity of mass-spectrometers is still increasing. Finally, exploring more mutations in the GTPases may identify GTP-locked or GDP-bound/empty forms that act more effectively to capture effectors or GEFs respectively. Indeed MitoID allows rapid testing of sequence variants - following transient transfection of variants, the biotinylated proteins can be isolated with streptavidin and probed by immunoblotting for known interactors. To illustrate this we tested the effect on Rab5A-GTP of mutations in Ser84 that has been identified as a potential site for phosphorylation (Steger et al., 2017; Ong et al., 2014). Mutating this to alanine or glutamate greatly reduced biotinylation of one effector (OSBPL9), but not others, suggesting that modification of this residue could differentially affect effector binding ((Figure 9-figure supplement 1C).

We anticipate that the MitoID approach, and the data presented in this paper, will be of help to many labs investigating small GTPases and potentially other families of proteins that function through transient interactions with cytosolic proteins.

Materials and Methods

Plasmids

For MitoID, Ras family GTPases lacking C-terminal cysteine residues and with mutations locking them in either the active or inactive conformation were cloned into pcDNA3.1$^+$ (Clontech), upstream of a GAGA linker. This was followed by the BirA* ligase, a second GAGAGA linker, a HA tag and residues 481-527 of monoamine oxidase (MAO) to target the construct to the mitochondria. The MitoID plasmids reported here are available from Addgene (https://www.addgene.org/Sean_Munro/ (to be released upon acceptance)).

Human STAMBPL1 was PCR amplified from FLAG-HA-STAMBPL1 (Addgene plasmid #22559), human TBC1 domain containing kinase (TBCK) was PCR amplified from Myc-DDK-tagged TBCK (transcript variant 4) (Insight Biotechnology Ltd, RC203605) and human Hermansky-Pudlak syndrome 3 (HPS3) from Myc-DDK-tagged HPS3 (Insight Biotechnology Ltd, RC204569). All were cloned between Not1 and XmaI downstream of FLAG or GFP-FLAG tags in pcDNA3.1$^+$. GFP-FLAG-constructs have a GAGAGA linker between the GFP and the FLAG tag. FLAG tag constructs have a GAGAGA linker and additional Prescission protease site the tag and the insert. ARFGEF3 was custom synthesized (Epoch Life Sciences) and cloned between KpnI and NotI into pcDNA3.1$^+$. FLAG or GFP-FLAG tags as above were PCR amplified and inserted upstream of the ARFGEF3 ORF between NheI and KpnI. Bacterial expression used *E.coli* codon-optimized human Rab constructs created by cloning Rab GTPases lacking the C-terminal cysteines and with the relevant activating or inactivating point mutations (see Table 1) into the vector pGEX6p2 between EcoR1 and XhoI (GE Healthcare Life Sciences). Full-length NDE1 was PCR amplified from the plasmid HG15586 (Stratech Scientific) and cloned between BamH1 and HindIII in *E. coli* expression vector p810 (Andrew Carter, MRC LMB Cambridge UK), thus adding an N-terminal His_6 tag followed by a dihydrolipoyl acetyltransferases solubility tag and a TEV cleavage site. The GFP-PX domain plasmid was provided by Yohei Ohashi (MRC LMB, Cambridge, UK).

Antibodies and probes

Antibodies used for immunofluorescence (IF) experiments in this study were: HA tag (Roche, 3F10/11 867 423 001), giantin (Santa Cruz, N-18/sc48363), COXIV (3E11) (New England Biolabs Ltd, 4850S), and ZFPL1 (Sigma, HPA014909). Antibodies for Western blotting were the same as those used for IF plus: GM130 (BD Transduction Labs, 610823), STAMBPL1 (Sigma, SAB4200146), NDE1 (Life Technologies, 711424), TBCK (Cambridge Bioscience, HPA039951), KIAA1468 (Cambridge Bioscience, HPA040038), OSBPL9 (Abcam, ab151691), PIK3R4 (Abcam, ab128903), FLAG (M2) (Sigma, F1804), EEA1 (Abcam, ab109110), ARFGEF3 (ThermoFisher Scientific, PA5-57623). Biotin was detected with Neutravidin-FITC (Invitrogen, 31006) and Streptavidin-HRP (Cell Signaling Technology, 3999S).

Cell culture and immunofluorescence

All cells were cultured in Dulbecco's modified Eagle's medium (DMEM; Invitrogen) supplemented with 10% fetal calf serum (FCS) and penicillin/streptomycin at 37°C and 5% CO2. For immunofluorescence experiments, HeLa cells (ATCC) were transfected with 1 µg of DNA and 4 µL FuGENE 6 in 100 µL Opti-MEM media for 24-36 hours according to the manufacturer's instructions (Promega). Cells were fixed with 4% (v/v) formaldehyde in PBS and permeabilized in 0.5% (v/v) Triton-X-100 in PBS. Cells were blocked for one hour in PBS containing 20% (v/v) FCS and 0.25% (v/v) Tween-20 and probed with the antibodies in the same buffer. Primary antibodies were detected with species-specific Alexa-labeled secondary antibodies (Molecular Probes). The cells were mounted in Vectashield (Vector Laboratories) and imaged using either an LSM 780 (Zeiss) or a TCS SP8 (Leica) confocal microscope.

Protein blotting

All blots, except for those with Streptavidin-HRP, were blocked in 5% (w/v) milk in PBS-T (PBS with 0.1% (v/v) Tween-20) for 30-60 min, incubated either for 1 h at room temperature or overnight at 4°C with primary antibody in the same blocking solution. Washed extensively with PBS-T then incubated with HRP-conjugated

secondary antibody in 0.1% (w/v) milk in PBS-T for one hour, washed again in PBS-T, then once in PBS only and detected with either Immobilon Western HRP substrate or Amersham ECL detection reagent. For probing with Streptavidin-HRP, the blots were blocked in 0.2% (w/v) I-BLOCK (Tropix, Applied Biosystems) in 0.1% PBS-T for 30-60 minutes. Primary and secondary antibodies were diluted using this blocking solution and incubated and processed as above.

Affinity capture of biotinylated proteins

The protocol for isolating proteins biotinylated by BirA* was adapted from the BioID method (Roux et al., 2012). Briefly, HEK293T cells were grown in two 175 cm^2 flasks to ~50% confluence and transfected with 25 µg plasmid and 75 µl FuGENE 6 in 2 ml Opti-MEM according to the manufacturers instructions (Promega). One day after transfection, biotin was added to 50 µM, and the cells incubated for a further 18 hours. Cells were pelleted by centrifugation (1000 x *g*, 5 min), washed once in ice-cold PBS and resuspended in lysis buffer (25 mM Tris pH 7.4, 150 mM NaCl, 1 mM EDTA, 1% (v/v) Triton X-100, 1 mM PMSF, 1 cOmplete protease inhibitor cocktail tablet (Roche)/50 ml buffer), and incubated for 30-60 min at 4°C with rotation. After centrifugation at 10,000 x *g* for 10 min at 4°C, the supernatants were added to 500 µl Dynabeads MyOne Streptavidin C1 beads (Invitrogen) that had been pre-washed twice in the same buffer. The beads were incubated at 4°C overnight, washed twice in Wash Buffer 1 (2% SDS PAGE, cOmplete inhibitors), three times in Wash Buffer 2 (1% (v/v) Triton X-100, 0.1% (w/v) deoxycholate, 500 mM NaCl, 1 mM EDTA, 50 mM HEPES, cOmplete inhibitors, pH 7.5), and three times in Wash Buffer 3 (50 mM Tris pH 7.4, 50 mM NaCl, cOmplete inhibitors). Finally, the beads were incubated in 75 µl SDS sample buffer containing 3 mM biotin at 98°C for 5 min to release the biotinylated proteins from the beads. 1 mM β-mercaptoethanol was then added to the SDS sample buffer and 20 µl of the sample analysed by SDS-PAGE and mass spectrometry with the remainder reserved for immunoblotting. All MitoID experiments were performed as biological replicates: the three experiments that

constitute a triplicate set for a given GTPase performed on cells transfected independently on different days and processed separately.

Mass spectrometry

Samples obtained from affinity chromatography and proximity biotinylation were loaded on 4-20% Tris-glycine SDS-PAGE gels and run for 1-2 centimeters. Proteins were stained with Coomassie InstantBlue (Expedeon), the protein-containing part of the gel lane cut into eight slices that were placed in a 96-well plate and destained with 50% v/v acetonitrile and 50 mM ammonium bicarbonate, reduced with 10 mM DTT, and alkylated with 55 mM iodoacetamide. Digestion was with 6 ng/µl trypsin (Promega, UK) overnight at 37°C, and peptides extracted in 2% v/v formic acid 2% v/v acetonitrile, and analysed by nano-scale capillary LC-MS/MS (Ultimate U3000 HPLC, Thermo Scientific Dionex) at a flow of ~ 300 nL/min. A C18 Acclaim PepMap100 5 µm, 100 µm x 20 mm nanoViper (Thermo Scientific Dionex), trapped the peptides prior to separation on a C18 Acclaim PepMap100 3 µm, 75 µm x 250 mm nanoViper. Peptides were eluted with an acetonitrile gradient. The analytical column outlet was interfaced via a nanoflow electrospray ionisation source with a linear ion trap mass spectrometer (Orbitrap Velos, Thermo Scientific). Data dependent analysis was performed using a resolution of 30,000 for the full MS spectrum, followed by ten MS/MS spectra in the linear ion trap. MS spectra were collected over a m/z range of 300–2000. MS/MS scans were collected using a threshold energy of 35 for collision-induced dissociation. The mass spectrometry data have been deposited to the ProteomeXchange Consortium via the PRIDE partner repository with the dataset identifier PRIDE: PXDXXXXXX (available to reviewers on request).

Analysis of mass spectrometry data

For analysis of spectral counts and calculation of WD scores LC-MS/MS data were searched against the manually reviewed UniProt human proteome using Mascot (Matrix Science), with a precursor tolerance of 5 ppm and a fragment ion mass

tolerance of 0.8 Da. The gene RABGAP1L, has two entries, RBG1L_HUMAN and RBG10_HUMAN, and so the latter as removed. Two missed enzyme cleavages and variable modifications for oxidised methionine, carbamidomethyl cysteine, pyroglutamic acid, phosphorylated serine, threonine and tyrosine were included. MS/MS data were validated using the Scaffold programme (Proteome Software Inc). To score the significance of interactors total spectral counts which were converted into D- and WD- scores according to the CompPASS methods (Sowa et al., 2009). The D-score assigns more confidence to proteins that are found in replicate experiments and that interact with fewer baits (in this case, fewer Rabs) and is, thus, a measure of specificity and reproducibility. The WD-score, in addition, takes into account that some preys (effectors) may interact with a subset of related baits (Rabs) and so in this case the total spectral counts found in this sub-set of baits will be higher than the general background level.

For analysis of spectral intensities and generation of volcano plots LC-MS/MS raw files were processed in MaxQuant (version1.6.2.6) and the peptide lists generated searched against the reviewed UniProt human proteome (as above) using the Andromeda search engine embedded in MaxQuant (Cox and Mann, 2008; Cox et al., 2011). Enzyme specificity for trypsin was selected (cleavage at the C-terminal side of lysine and arginine amino acid residues, unless proline is present on the carboxyl side of the cleavage site) and a maximum of two missed cleavages were allowed. Cysteine carbamidomethylation was set as a fixed modification, while phosphorylation of serine, threonine and tyrosine, and oxidation of methionine were set as variable modifications. Peptides were identified with an initial precursor mass deviation of up to 10 ppm and a fragment mass deviation of 0.2 Da. For label-free protein quantitation (MaxLFQ) we required a minimum ratio count of 1, with two minimum and two average comparisons, which enabled normalization of this large dataset (Hein et al., 2015). A false discovery rate (FDR), determined by searching a reverse sequence database, of 0.01 was used at both the protein and peptide level.

Data from the Maxquant analysis was analysed on the Perseus platform (Tyanova et al., 2016). Protein identifications were filtered, removing hits to the

reverse decoy database as well as proteins only identified by modified peptides. We required that each protein be detected in at least two out of the three replicates from the AP-MS samples of at least one bait. Protein LFQ intensities were logarithmized and missing values imputed by values simulating noise around the detection limit using the Perseus default settings (Tyanova et al., 2016). To calculate p-values two sample Student's t-tests were performed in which baits were compared against the entire dataset of GDP-locked GTPases with the number of randomizations set at 250.

Immunoprecipitation of FLAG-tagged STAMBPL1 from HEK293T cells

Three 175 cm^2 flasks of HEK293T cells (ATCC) at 60-70% confluence were transfected with plasmids encoding GFP-FLAG tagged STAMBPL1 using FuGENE 6 according to the manufacturers instructions. After 48 h cells were harvested by centrifugation, washed once in ice-cold PBS and lysed in lysis buffer (25 mM Tris-HCl pH7.4m 150 mM NaCl, 1 mM EDTA, 0.5% (V/V) Triton X-100, 1 EDTA-free complete protease inhibitor tablet/50 ml, 1 mM PMSF) for 30 min at 4°C. Lysates were clarified by centrifugation before GFP-FLAG-tagged proteins were isolated by incubation with 100 µL packed FLAG M2 affinity resin (Sigma) for 1 h with rotation at 4°C. Beads were washed extensively in lysis buffer and bound proteins eluted in 500 µL 100 µg/ml 3X FLAG peptide (Sigma) in 25 mM Tris-HCl pH 7.4, 250 mM NaCl, 1 mM EDTA.

Affinity chromatography of GST-Rab2A and Rab5A with purified GFP-FLAG-STAMBPL1

Rab2A with Q65L (GTP-locked) or S20N (GFP-locked) mutations and Rab5A with Q79L (GTP-locked) or S34N (GFP-locked) mutations were expressed in *E. coli* strain BL21-GOLD (DE3; Agilent Technologies) as fusions to GST. Bacteria were grown at 37°C to an OD_{600} of 0.7 and induced with 100 µM IPTG overnight at 16°C. Cells were harvested by centrifugation, dounce homogenized and sonicated in lysis buffer (50 mM Tris-HCl, pH 7.4, 150 mM NaCl, 5 mM $MgCl_2$, 1% Triton X-100, 5 mM β-

mercaptoethanol, plus 1 EDTA-free complete protease tablet/50 ml, 1 mM PMSF and either 100 μM non-hydrolyzable GTP analogue (GppNHp, Sigma) or 100 μM GDP as appropriate). The lysates were clarified by centrifugation at 12,000 x *g* for 15 min and GST-Rab proteins were applied at saturating levels to glutathione Sepharose beads (GE Healthcare) for 30 min at 4°C and then washed extensively to remove unbound material. 100 μl of purified GFP-FLAG-STAMBPL1 was applied to 50 μl of GST-Rab beads in 500 μl lysis buffer plus 100 μM GppNHp or GDP as required, and rotated at 4°C for 2 h. Beads were then washed in lysis buffer containing 100 μM of the relevant nucleotide before bound proteins were eluted in high salt buffer (25 mM Tris-HCL, pH7.4, 1.5 M NaCl, 20 mM EDTA, 5 mM β-mercaptoethanol and 1 mM of the opposing nucleotide). Proteins were precipitated with chloroform/methanol, resuspended in SDS sample buffer with 1 mM β-mercaptoethanol and analysed by SDS-PAGE.

Affinity chromatography of *E. coli* expressed GST-Rab9A and His6-tagged NDE1

Rab9A bearing Q66L or S21N mutations was expressed in the *E. coli* strain BL21-GOLD (DE3; Agilent Technologies) as a fusion to GST. NDE1 was expressed in the same bacteria as a fusion to a N-terminal His_6 tag with a dihydrolipoyl acetyltransferase solubility tag and a TEV cleavage site between the His_6 tag and the NDE1 insert. Bacteria were grown, harvested, lysed and the GST-Rab9A proteins applied to glutathione-Sepharose beads as described above for GST-Rab2A and GST-Rab5A. Lysates containing NDE1 were also incubated with glutathione-Sepharose beads to pre-clear the sample prior to incubation with 50 μl GST-Rab coated beads for 2 h with rotation at 4°C. Beads and protein complexes were washed extensively in lysis buffer and proteins were eluted in SDS sample buffer with 1 mM β-mercaptoethanol. Lysates and eluates were separated by SDS-PAGE electrophoresis and analysed either by mass spectrometry or by transfer to nitrocellulose and probing with antibodies.

Affinity chromatography of cell lysates using GST-Rab2A, 5A, 6A, 9A and 11A

GST-Rab proteins were expressed and purified from the *E. coli* strain BL21-GOLD (DE3; Agilent Technologies) as described above. HEK293T cells from 5 x T175 cm flasks were collected, washed and lysed in 10 ml of lysis buffer (25 mM Tris-HCl, pH 7.4, 150 mM NaCl, 5 mM $MgCl_2$, 1% Triton X-100, 5 mM β -mercaptoethanol, plus 1 EDTA-free complete protease tablet/50 ml and 1 mM PMSF). The lysate was divided equally and applied to 50 µl of GST-Rab coated beads with either 100 µM non-hydrolyzable GTP (GppNHp) or 100 µM GDP added as appropriate. Beads were incubated, washed and proteins eluted in high salt buffer as described above. Proteins were precipitated and analyzed by immunoblotting with the indicated antibodies. As we found no suitable antibody for HPS3, 1 x T175cm^2 flask of HEK293T cells was transfected with FLAG-tagged HPS3 using Fugene 6 and 24 h later cells were lysed and incubated with GST-Rab as for the untransfected lysate. In the case of ARFGEF3 rat brain was used as a source of the endogenous material. The brain was harvested rapidly and placed into ice-cold PBS. Following several washes in PBS, the brain was minced into small pieces and 10 volumes (50 ml) of lysis buffer added (20 mM Tris-HCl, pH8, 150 mM KCl, 5 mM $MgCl_2$, 1 mM PMSF, 1% (w/v) CHAPS, plus 1 EDTA-free complete protease tablet/25 ml buffer). The material was dounce homogenized, solubilized by rotation at 4°C for 3 h and centrifuged at 100,000 x *g* for 60 min at 4°C. The supernatant was stored in aliquots at -80°C. For each Rab affinity chromatography experiment five ml of supernatant was applied to 50 ml of Rab saturated glutathione Sepharose beads. The beads were then incubated and processed as already described except 1% (w/v) CHAPS replaced Triton X-100 in the wash buffer.

Acknowledgements

We thank Alan Gillingham, Harriet Parsons, Mark Skehel and Tim Stevens for help with computational analysis of mass-spectrometry data; and Andrew Carter and Yohei Ohashi for reagents. This work was supported by the Medical Research Council (MRC file reference number MC_U105178783).

References

Ailion, M., M. Hannemann, S. Dalton, A. Pappas, S. Watanabe, J. Hegermann, Q. Liu, H.-F. Han, M. Gu, M.Q. Goulding, N. Sasidharan, K. Schuske, P. Hullett, S. Eimer, and E.M. Jorgensen. 2014. Two Rab2 interactors regulate dense-core vesicle maturation. *Neuron*. 82:167–180. doi:10.1016/j.neuron.2014.02.017.

Barker, A.R., K.V. McIntosh, and H.R. Dawe. 2016. Centrosome positioning in non-dividing cells. *Protoplasma*. 253:1007–1021. doi:10.1007/s00709-015-0883-5.

Barr, F., and D.G. Lambright. 2010. Rab GEFs and GAPs. *Curr Opin Cell Biol*. 22:461–470. doi:10.1016/j.ceb.2010.04.007.

Beer, K.B., J. Rivas-Castillo, K. Kuhn, G. Fazeli, B. Karmann, J.F. Nance, C. Stigloher, and A.M. Wehman. 2018. Extracellular vesicle budding is inhibited by redundant regulators of TAT-5 flippase localization and phospholipid asymmetry. *Proc Natl Acad Sci U S A*. 115:E1127–E1136. doi:10.1073/pnas.1714085115.

Behrends, C., M.E. Sowa, S.P. Gygi, and J.W. Harper. 2010. Network organization of the human autophagy system. *Nature*. 466:68–76. doi:10.1038/nature09204.

Bradshaw, N.J., and M.A.F. Hayashi. 2017. NDE1 and NDEL1 from genes to (mal)functions: parallel but distinct roles impacting on neurodevelopmental disorders and psychiatric illness. *Cell Mol Life Sci*. 74:1191–1210. doi:10.1007/s00018-016-2395-7.

Branon, T.C., J.A. Bosch, A.D. Sanchez, N.D. Udeshi, T. Svinkina, S.A. Carr, J.L. Feldman, N. Perrimon, and A.Y. Ting. 2018. Efficient proximity labeling in living cells and organisms with TurboID. *Nat Biotechnol*. 36:880–887. doi:10.1038/nbt.4201.

Brooks, S.P., M. Coccia, H.R. Tang, N. Kanuga, L.M. Machesky, M. Bailly, M.E. Cheetham, and A.J. Hardcastle. 2010. The Nance-Horan syndrome protein encodes a functional WAVE homology domain (WHD) and is important for co-ordinating actin remodelling and maintaining cell morphology. *Hum Mol Genet*. 19:2421–2432. doi:10.1093/hmg/ddq125.

Buffa, L., E. Fuchs, M. Pietropaolo, F. Barr, and M. Solimena. 2008. ICA69 is a novel Rab2 effector regulating ER-Golgi trafficking in insulinoma cells. *Eur J Cell Biol*. 87:197–209. doi:10.1016/j.ejcb.2007.11.003.

Burke, J.E., A.J. Inglis, O. Perisic, G.R. Masson, S.H. McLaughlin, F. Rutaganira, K.M. Shokat, and R.L. Williams. 2014. Structures of PI4KIIIβ complexes show simultaneous recruitment of Rab11 and its effectors. *Science*. 344:1035–1038. doi:10.1126/science.1253397.

Casanova, J.E., and B. Winckler. 2017. A new Rab7 effector controls phosphoinositide conversion in endosome maturation. *J Cell Biol*. 216:2995–2997. doi:10.1083/jcb.201709034.

Cherfils, J., and M. Zeghouf. 2013. Regulation of small GTPases by GEFs, GAPs, and GDIs. *Physiol Rev*. 93:269–309. doi:10.1152/physrev.00003.2012.

Chong, J.X., V. Caputo, I.G. Phelps, L. Stella, L. Worgan, J.C. Dempsey, A. Nguyen, V. Leuzzi, R. Webster, A. Pizzuti, C.T. Marvin, G.E. Ishak, S. Ardern-Holmes, Z.

Richmond, University of Washington Center for Mendelian Genomics, M.J. Bamshad, X.R. Ortiz-Gonzalez, M. Tartaglia, M. Chopra, and D. Doherty. 2016. Recessive Inactivating Mutations in TBCK, Encoding a Rab GTPase-Activating Protein, Cause Severe Infantile Syndromic Encephalopathy. *Am J Hum Genet*. 98:772–781. doi:10.1016/j.ajhg.2016.01.016.

Christoforidis, S., H.M. McBride, R.D. Burgoyne, and M. Zerial. 1999a. The Rab5 effector EEA1 is a core component of endosome docking. *Nature*. 397:621–625. doi:10.1038/17618.

Christoforidis, S., M. Miaczynska, K. Ashman, M. Wilm, L. Zhao, S.C. Yip, M.D. Waterfield, J.M. Backer, and M. Zerial. 1999b. Phosphatidylinositol-3-OH kinases are Rab5 effectors. *Nat Cell Biol*. 1:249–252. doi:10.1038/12075.

Clague, M.J., and S. Urbé. 2006. Endocytosis: the DUB version. *Trends Cell Biol*. 16:551–559. doi:10.1016/j.tcb.2006.09.002.

Colicelli, J. 2004. Human RAS superfamily proteins and related GTPases. *Sci. STKE*. 2004:RE13. doi:10.1126/stke.2502004re13.

Cox, J., and M. Mann. 2008. MaxQuant enables high peptide identification rates, individualized p.p.b.-range mass accuracies and proteome-wide protein quantification. *Nat Biotechnol*. 26:1367–1372. doi:10.1038/nbt.1511.

Cox, J., N. Neuhauser, A. Michalski, R.A. Scheltema, J.V. Olsen, and M. Mann. 2011. Andromeda: a peptide search engine integrated into the MaxQuant environment. *J Proteome Res*. 10:1794–1805. doi:10.1021/pr101065j.

Csizmadia, T., P. Lorincz, K. Hegedűs, S. Széplaki, P. Lőw, and G. Juhasz. 2018. Molecular mechanisms of developmentally programmed crinophagy in *Drosophila*. *J Cell Biol*. 217:361–374. doi:10.1083/jcb.201702145.

Cuif, M.H., F. Possmayer, H. Zander, N. Bordes, F. Jollivet, A. Couedel-Courteille, I. Janoueix-Lerosey, G. Langsley, M. Bornens, and B. Goud. 1999. Characterization of GAPCenA, a GTPase activating protein for Rab6, part of which associates with the centrosome. *EMBO J*. 18:1772–1782. doi:10.1093/emboj/18.7.1772.

Dejgaard, S.Y., A. Murshid, A. Erman, O. Kizilay, D. Verbich, R. Lodge, K. Dejgaard, T.B.N. Ly-Hartig, R. Pepperkok, J.C. Simpson, and J.F. Presley. 2008. Rab18 and Rab43 have key roles in ER-Golgi trafficking. *J Cell Sci*. 121:2768–2781. doi:10.1242/jcs.021808.

Dennis, M.K., A.R. Mantegazza, O.L. Snir, D. Tenza, A. Acosta-Ruiz, C. Delevoye, R. Zorger, A. Sitaram, W. de Jesus-Rojas, K. Ravichandran, J. Rux, E.V. Sviderskaya, D.C. Bennett, G. Raposo, M.S. Marks, and S.R.G. Setty. 2015. BLOC-2 targets recycling endosomal tubules to melanosomes for cargo delivery. *J Cell Biol*. 209:563–577. doi:10.1083/jcb.201410026.

Der, C.J., T. Finkel, and G.M. Cooper. 1986. Biological and biochemical properties of human rasH genes mutated at codon 61. *Cell*. 44:167–176.

Dong, R., Y. Saheki, S. Swarup, L. Lucast, J.W. Harper, and P. De Camilli. 2016. Endosome-ER Contacts Control Actin Nucleation and Retromer Function

through VAP-Dependent Regulation of PI4P. *Cell*. 166:408–423. doi:10.1016/j.cell.2016.06.037.

Eathiraj, S., X. Pan, C. Ritacco, and D.G. Lambright. 2005. Structural basis of family-wide Rab GTPase recognition by rabenosyn-5. *Nature*. 436:415–419. doi:10.1038/nature03798.

Eggers, C.T., J.C. Schafer, J.R. Goldenring, and S.S. Taylor. 2009. D-AKAP2 interacts with Rab4 and Rab11 through its RGS domains and regulates transferrin receptor recycling. *J Biol Chem*. 284:32869–32880. doi:10.1074/jbc.M109.022582.

Elias, M., A. Brighouse, C. Gabernet-Castello, M.C. Field, and J.B. Dacks. 2012. Sculpting the endomembrane system in deep time: high resolution phylogenetics of Rab GTPases. *J Cell Sci*. 125:2500–2508. doi:10.1242/jcs.101378.

Etoh, K., and M. Fukuda. 2019. Rab10 regulates tubular endosome formation through KIF13A/B motors. *J Cell Sci*. jcs.226977. doi:10.1242/jcs.226977.

Feig, L.A. 1999. Tools of the trade: use of dominant-inhibitory mutants of Ras-family GTPases. *Nat Cell Biol*. 1:E25–7. doi:10.1038/10018.

Fridmann-Sirkis, Y., S. Siniossoglou, and H.R.B. Pelham. 2004. TMF is a golgin that binds Rab6 and influences Golgi morphology. *BMC Cell Biol*. 5:18. doi:10.1186/1471-2121-5-18.

Fuchs, E., A.K. Haas, R.A. Spooner, S.-I. Yoshimura, J.M. Lord, and F.A. Barr. 2007. Specific Rab GTPase-activating proteins define the Shiga toxin and epidermal growth factor uptake pathways. *J Cell Biol*. 177:1133–1143. doi:10.1083/jcb.200612068.

Fukuda, M., E. Kanno, C. Saegusa, Y. Ogata, and T.S. Kuroda. 2002. Slp4-a/granuphilin-a regulates dense-core vesicle exocytosis in PC12 cells. *J Biol Chem*. 277:39673–39678. doi:10.1074/jbc.M205349200.

Fukuda, M., E. Kanno, K. Ishibashi, and T. Itoh. 2008. Large scale screening for novel rab effectors reveals unexpected broad Rab binding specificity. *Mol Cell Proteomics*. 7:1031–1042. doi:10.1074/mcp.M700569-MCP200.

Fukuda, M., H. Kobayashi, K. Ishibashi, and N. Ohbayashi. 2011. Genome-wide investigation of the Rab binding activity of RUN domains: development of a novel tool that specifically traps GTP-Rab35. *Cell Struct Funct*. 36:155–170.

Gadea, G., and A. Blangy. 2014. Dock-family exchange factors in cell migration and disease. *Eur J Cell Biol*. 93:466–477. doi:10.1016/j.ejcb.2014.06.003.

Gautam, R., S. Chintala, W. Li, Q. Zhang, J. Tan, E.K. Novak, S.M. Di Pietro, E.C. Dell'Angelica, and R.T. Swank. 2004. The Hermansky-Pudlak syndrome 3 (cocoa) protein is a component of the biogenesis of lysosome-related organelles complex-2 (BLOC-2). *J Biol Chem*. 279:12935–12942. doi:10.1074/jbc.M311311200.

Gentry, L.R., T.D. Martin, D.J. Reiner, and C.J. Der. 2014. Ral small GTPase signaling and oncogenesis: More than just 15minutes of fame. *Biochim Biophys*

Acta. 1843:2976–2988. doi:10.1016/j.bbamcr.2014.09.004.

Gerondopoulos, A., R.N. Bastos, S.-I. Yoshimura, R. Anderson, S. Carpanini, I. Aligianis, M.T. Handley, and F.A. Barr. 2014. Rab18 and a Rab18 GEF complex are required for normal ER structure. *J Cell Biol*. 205:707–720. doi:10.1083/jcb.201403026.

Gillingham, A.K., R. Sinka, I.L. Torres, K.S. Lilley, and S. Munro. 2014. Toward a comprehensive map of the effectors of Rab GTPases. *Dev Cell*. 31:358–373. doi:10.1016/j.devcel.2014.10.007.

Grigoriev, I., D. Splinter, N. Keijzer, P.S. Wulf, J. Demmers, T. Ohtsuka, M. Modesti, I.V. Maly, F. Grosveld, C.C. Hoogenraad, and A. Akhmanova. 2007. Rab6 regulates transport and targeting of exocytotic carriers. *Dev Cell*. 13:305–314. doi:10.1016/j.devcel.2007.06.010.

Grigoriev, I., K.L. Yu, E. Martinez-Sanchez, A. Serra-Marques, I. Smal, E. Meijering, J. Demmers, J. Peränen, R.J. Pasterkamp, P. van der Sluijs, C.C. Hoogenraad, and A. Akhmanova. 2011. Rab6, Rab8, and MICAL3 cooperate in controlling docking and fusion of exocytotic carriers. *Curr. Biol.* 21:967–974. doi:10.1016/j.cub.2011.04.030.

Hayes, G.L., F.C. Brown, A.K. Haas, R.M. Nottingham, F.A. Barr, and S.R. Pfeffer. 2009. Multiple Rab GTPase binding sites in GCC185 suggest a model for vesicle tethering at the trans-Golgi. *Mol Biol Cell*. 20:209–217. doi:10.1091/mbc.E08-07-0740.

Heard, J.J., V. Fong, S.Z. Bathaie, and F. Tamanoi. 2014. Recent progress in the study of the Rheb family GTPases. *Cell. Signal.* 26:1950–1957. doi:10.1016/j.cellsig.2014.05.011.

Heasman, S.J., and A.J. Ridley. 2008. Mammalian Rho GTPases: new insights into their functions from in vivo studies. *Nat Rev Mol Cell Biol*. 9:690–701. doi:10.1038/nrm2476.

Hein, M.Y., N.C. Hubner, I. Poser, J. Cox, N. Nagaraj, Y. Toyoda, I.A. Gak, I. Weisswange, J. Mansfeld, F. Buchholz, A.A. Hyman, and M. Mann. 2015. A human interactome in three quantitative dimensions organized by stoichiometries and abundances. *Cell*. 163:712–723. doi:10.1016/j.cell.2015.09.053.

Hobbs, G.A., C.J. Der, and K.L. Rossman. 2016. RAS isoforms and mutations in cancer at a glance. *J Cell Sci*. 129:1287–1292. doi:10.1242/jcs.182873.

Hoogenraad, C.C., I. Popa, K. Futai, E. Martinez-Sanchez, E. Sanchez-Martinez, P.S. Wulf, T. van Vlijmen, B.R. Dortland, V. Oorschot, R. Govers, M. Monti, A.J.R. Heck, M. Sheng, J. Klumperman, H. Rehmann, D. Jaarsma, L.C. Kapitein, and P. van der Sluijs. 2010. Neuron specific Rab4 effector GRASP-1 coordinates membrane specialization and maturation of recycling endosomes. *PLoS Biol*. 8:e1000283. doi:10.1371/journal.pbio.1000283.

Hoogenraad, C.C., P. Wulf, N. Schiefermeier, T. Stepanova, N. Galjart, J.V. Small, F. Grosveld, C.I. De Zeeuw, and A. Akhmanova. 2003. Bicaudal D induces selective dynein-mediated microtubule minus end-directed transport. *EMBO J*. 22:6004–

6015. doi:10.1093/emboj/cdg592.

Horiuchi, H., R. Lippé, H.M. McBride, M. Rubino, P. Woodman, H. Stenmark, V. Rybin, M. Wilm, K. Ashman, M. Mann, and M. Zerial. 1997. A novel Rab5 GDP/GTP exchange factor complexed to Rabaptin-5 links nucleotide exchange to effector recruitment and function. *Cell*. 90:1149–1159.

Hua, K., and R.J. Ferland. 2018. Primary cilia proteins: ciliary and extraciliary sites and functions. *Cell Mol Life Sci*. 75:1521–1540. doi:10.1007/s00018-017-2740-5.

Hutagalung, A.H., and P.J. Novick. 2011. Role of Rab GTPases in membrane traffic and cell physiology. *Physiol Rev*. 91:119–149. doi:10.1152/physrev.00059.2009.

Huttlin, E.L., L. Ting, R.J. Bruckner, F. Gebreab, M.P. Gygi, J. Szpyt, S. Tam, G. Zarraga, G. Colby, K. Baltier, R. Dong, V. Guarani, L.P. Vaites, A. Ordureau, R. Rad, B.K. Erickson, M. Wühr, J. Chick, B. Zhai, D. Kolippakkam, J. Mintseris, R.A. Obar, T. Harris, S. Artavanis-Tsakonas, M.E. Sowa, P. De Camilli, J.A. Paulo, J.W. Harper, and S.P. Gygi. 2015. The BioPlex Network: a systematic exploration of the human interactome. *Cell*. 162:425–440. doi:10.1016/j.cell.2015.06.043.

Huttlin, E.L., R.J. Bruckner, J.A. Paulo, J.R. Cannon, L. Ting, K. Baltier, G. Colby, F. Gebreab, M.P. Gygi, H. Parzen, J. Szpyt, S. Tam, G. Zarraga, L. Pontano-Vaites, S. Swarup, A.E. White, D.K. Schweppe, R. Rad, B.K. Erickson, R.A. Obar, K.G. Guruharsha, K. Li, S. Artavanis-Tsakonas, S.P. Gygi, and J.W. Harper. 2017. Architecture of the human interactome defines protein communities and disease networks. *Nature*. 545:505–509. doi:10.1038/nature22366.

Itoh, T., M. Satoh, E. Kanno, and M. Fukuda. 2006. Screening for target Rabs of TBC (Tre-2/Bub2/Cdc16) domain-containing proteins based on their Rab-binding activity. *Genes Cells*. 11:1023–1037. doi:10.1111/j.1365-2443.2006.00997.x.

Itzen, A., and R.S. Goody. 2011. GTPases involved in vesicular trafficking: structures and mechanisms. *Semin Cell Dev Biol*. 22:48–56. doi:10.1016/j.semcdb.2010.10.003.

John, J., H. Rensland, I. Schlichting, I. Vetter, G.D. Borasio, R.S. Goody, and A. Wittinghofer. 1993. Kinetic and structural analysis of the Mg(2+)-binding site of the guanine nucleotide-binding protein p21H-ras. *J Biol Chem*. 268:923–929.

Keilhauer, E.C., M.Y. Hein, and M. Mann. 2015. Accurate protein complex retrieval by affinity enrichment mass spectrometry (AE-MS) rather than affinity purification mass spectrometry (AP-MS). *Mol Cell Proteomics*. 14:120–135. doi:10.1074/mcp.M114.041012.

Kelly, E.E., F. Giordano, C.P. Horgan, F. Jollivet, G. Raposo, and M.W. McCaffrey. 2012. Rab30 is required for the morphological integrity of the Golgi apparatus. *Biol Cell*. 104:84–101. doi:10.1111/boc.201100080.

Kim, D.I., S.C. Jensen, K.A. Noble, B. Kc, K.H. Roux, K. Motamedchaboki, and K.J. Roux. 2016. An improved smaller biotin ligase for BioID proximity labeling. *Mol Biol Cell*. 27:1188–1196. doi:10.1091/mbc.E15-12-0844.

Kloepper, T., N. Kienle, D. Fasshauer, and S. Munro. 2012. Untangling the evolution of Rab G proteins: implications of a comprehensive genomic analysis. *BMC Biol*. 10:71. doi:10.1186/1741-7007-10-71.

Knödler, A., S. Feng, J. Zhang, X. Zhang, A. Das, J. Peränen, and W. Guo. 2010. Coordination of Rab8 and Rab11 in primary ciliogenesis. *Proc Natl Acad Sci U S A*. 107:6346–6351. doi:10.1073/pnas.1002401107.

Koch, D., A. Rai, I. Ali, N. Bleimling, T. Friese, A. Brockmeyer, P. Janning, B. Goud, A. Itzen, M.P. Müller, and R.S. Goody. 2016. A pull-down procedure for the identification of unknown GEFs for small GTPases. *smallgtpases*. 7:93–106. doi:10.1080/21541248.2016.1156803.

Laflamme, C., G. Assaker, D. Ramel, J.F. Dorn, D. She, P.S. Maddox, and G. Emery. 2012. Evi5 promotes collective cell migration through its Rab-GAP activity. *J Cell Biol*. 198:57–67. doi:10.1083/jcb.201112114.

Lam, C., M.A.S. Vergnolle, L. Thorpe, P.G. Woodman, and V.J. Allan. 2010. Functional interplay between LIS1, NDE1 and NDEL1 in dynein-dependent organelle positioning. *J Cell Sci*. 123:202–212. doi:10.1242/jcs.059337.

Lambert, J.-P., M. Tucholska, C. Go, J.D.R. Knight, and A.-C. Gingras. 2015. Proximity biotinylation and affinity purification are complementary approaches for the interactome mapping of chromatin-associated protein complexes. *J Proteomics*. 118:81–94. doi:10.1016/j.jprot.2014.09.011.

Langemeyer, L., R. Nunes-Bastos, Y. Cai, A. Itzen, K.M. Reinisch, and F.A. Barr. 2014. Diversity and plasticity in Rab GTPase nucleotide release mechanism has consequences for Rab activation and inactivation. *eLife*. 3:e01623.

Li, G., and P.D. Stahl. 1993. Structure-function relationship of the small GTPase rab5. *J Biol Chem*. 268:24475–24480.

Li, H., S. Wei, K. Cheng, N.V. Gounko, R.E. Ericksen, A. Xu, W. Hong, and W. Han. 2014. BIG3 inhibits insulin granule biogenesis and insulin secretion. *EMBO Rep*. 15:714–722. doi:10.1002/embr.201338181.

Liao, Y., K. Kariya, C.D. Hu, M. Shibatohge, M. Goshima, T. Okada, Y. Watari, X. Gao, T.G. Jin, Y. Yamawaki-Kataoka, and T. Kataoka. 1999. RA-GEF, a novel Rap1A guanine nucleotide exchange factor containing a Ras/Rap1A-associating domain, is conserved between nematode and humans. *J Biol Chem*. 274:37815–37820.

Liu, L., C. Yang, J. Yuan, X. Chen, J. Xu, Y. Wei, J. Yang, G. Lin, and L. Yu. 2005. RPK118, a PX domain-containing protein, interacts with peroxiredoxin-3 through pseudo-kinase domains. *Mol. Cells*. 19:39–45.

Liu, Z., Y. Zhan, Y. Tu, K. Chen, Z. Liu, and C. Wu. 2015. PDZ and LIM domain protein 1(PDLIM1)/CLP36 promotes breast cancer cell migration, invasion and metastasis through interaction with α-actinin. *Oncogene*. 34:1300–1311. doi:10.1038/onc.2014.64.

Longatti, A., C.A. Lamb, M. Razi, S.-I. Yoshimura, F.A. Barr, and S.A. Tooze. 2012. TBC1D14 regulates autophagosome formation via Rab11- and ULK1-positive

recycling endosomes. *J Cell Biol*. 197:659–675. doi:10.1083/jcb.201111079.

Mahanty, S., K. Ravichandran, P. Chitirala, J. Prabha, R.A. Jani, and S.R.G. Setty. 2016. Rab9A is required for delivery of cargo from recycling endosomes to melanosomes. *Pigment Cell Melanoma Res*. 29:43–59. doi:10.1111/pcmr.12434.

Maldonado, M.D.M., and S. Dharmawardhane. 2018. Targeting Rac and Cdc42 GTPases in Cancer. *Cancer Res*. 78:3101–3111. doi:10.1158/0008-5472.CAN-18-0619.

Manning, B.D., and L.C. Cantley. 2003. Rheb fills a GAP between TSC and TOR. *Trends Biochem Sci*. 28:573–576. doi:10.1016/j.tibs.2003.09.003.

Martell, J.D., T.J. Deerinck, Y. Sancak, T.L. Poulos, V.K. Mootha, G.E. Sosinsky, M.H. Ellisman, and A.Y. Ting. 2012. Engineered ascorbate peroxidase as a genetically encoded reporter for electron microscopy. *Nat Biotechnol*. 30:1143–1148. doi:10.1038/nbt.2375.

Matanis, T., A. Akhmanova, P. Wulf, E. Del Nery, T. Weide, T. Stepanova, N. Galjart, F. Grosveld, B. Goud, C.I. De Zeeuw, A. Barnekow, and C.C. Hoogenraad. 2002. Bicaudal-D regulates COPI-independent Golgi-ER transport by recruiting the dynein-dynactin motor complex. *Nat Cell Biol*. 4:986–992. doi:10.1038/ncb891.

Medina, F., A.M. Carter, O. Dada, S. Gutowski, J. Hadas, Z. Chen, and P.C. Sternweis. 2013. Activated RhoA is a positive feedback regulator of the Lbc family of Rho guanine nucleotide exchange factor proteins. *J Biol Chem*. 288:11325–11333. doi:10.1074/jbc.M113.450056.

Merithew, E., S. Hatherly, J.J. Dumas, D.C. Lawe, R. Heller-Harrison, and D.G. Lambright. 2001. Structural plasticity of an invariant hydrophobic triad in the switch regions of Rab GTPases is a determinant of effector recognition. *J Biol Chem*. 276:13982–13988. doi:10.1074/jbc.M009771200.

Mitoma, J., and A. Ito. 1992. Mitochondrial targeting signal of rat liver monoamine oxidase B is located at its carboxy terminus. *J Biochem*. 111:20–24.

Müller, M.P., and R.S. Goody. 2018. Molecular control of Rab activity by GEFs, GAPs and GDI. *smallgtpases*. 9:5–21. doi:10.1080/21541248.2016.1276999.

Nakazawa, T., A.M. Watabe, T. Tezuka, Y. Yoshida, K. Yokoyama, H. Umemori, A. Inoue, S. Okabe, T. Manabe, and T. Yamamoto. 2003. p250GAP, a novel brain-enriched GTPase-activating protein for Rho family GTPases, is involved in the N-methyl-d-aspartate receptor signaling. *Mol Biol Cell*. 14:2921–2934. doi:10.1091/mbc.e02-09-0623.

Narumiya, S., and D. Thumkeo. 2018. Rho signaling research: history, current status and future directions. *FEBS Lett*. 592:1763–1776. doi:10.1002/1873-3468.13087.

Ngo, M., and N.D. Ridgway. 2009. Oxysterol binding protein-related Protein 9 (ORP9) is a cholesterol transfer protein that regulates Golgi structure and function. *Mol Biol Cell*. 20:1388–1399. doi:10.1091/mbc.E08-09-0905.

Nielsen, E., S. Christoforidis, S. Uttenweiler-Joseph, M. Miaczynska, F. Dewitte, M. Wilm, B. Hoflack, and M. Zerial. 2000. Rabenosyn-5, a novel Rab5 effector, is complexed with hVPS45 and recruited to endosomes through a FYVE finger

domain. *J Cell Biol*. 151:601–612.

Nigorikawa, K., K. Hazeki, J. Sasaki, Y. Omori, M. Miyake, S. Morioka, Y. Guo, T. Sasaki, and O. Hazeki. 2015. Inositol Polyphosphate-4-Phosphatase Type I Negatively Regulates Phagocytosis via Dephosphorylation of Phagosomal PtdIns(3,4)P2. *PLoS ONE*. 10:e0142091. doi:10.1371/journal.pone.0142091.

O'Loughlin, T., T.A. Masters, and F. Buss. 2018. The MYO6 interactome reveals adaptor complexes coordinating early endosome and cytoskeletal dynamics. *EMBO Rep*. 19:e44884. doi:10.15252/embr.201744884.

Oguchi, M.E., K. Noguchi, and M. Fukuda. 2017. TBC1D12 is a novel Rab11-binding protein that modulates neurite outgrowth of PC12 cells. *PLoS ONE*. 12:e0174883. doi:10.1371/journal.pone.0174883.

Ong, S.T., M. Freeley, J. Skubis-Zegadło, M.H.U.T. Fazil, D. Kelleher, F. Fresser, G. Baier, N.K. Verma, and A. Long. 2014. Phosphorylation of Rab5a protein by protein kinase Cϵ is crucial for T-cell migration. *J Biol Chem*. 289:19420–19434. doi:10.1074/jbc.M113.545863.

Otto, G.P., M. Razi, J. Morvan, F. Stenner, and S.A. Tooze. 2010. A novel syntaxin 6-interacting protein, SHIP164, regulates syntaxin 6-dependent sorting from early endosomes. *Traffic*. 11:688–705. doi:10.1111/j.1600-0854.2010.01049.x.

Paul, F., H. Zauber, L. von Berg, O. Rocks, O. Daumke, and M. Selbach. 2017. Quantitative GTPase Affinity Purification Identifies Rho Family Protein Interaction Partners. *Mol Cell Proteomics*. 16:73–85. doi:10.1074/mcp.M116.061531.

Pfeffer, S.R. 2011. Entry at the trans-face of the Golgi. *Cold Spring Harb Perspect Biol*. 3:a005272. doi:10.1101/cshperspect.a005272.

Pinkas, D.M., C.E. Sanvitale, J.C. Bufton, F.J. Sorrell, N. Solcan, R. Chalk, J. Doutch, and A.N. Bullock. 2017. Structural complexity in the KCTD family of Cullin3-dependent E3 ubiquitin ligases. *Biochem J*. 474:3747–3761. doi:10.1042/BCJ20170527.

Rai, A., A. Oprisko, J. Campos, Y. Fu, T. Friese, A. Itzen, R.S. Goody, E.-M. Gazdag, and M.P. Müller. 2016. bMERB domains are bivalent Rab8 family effectors evolved by gene duplication. *eLife*. 5. doi:10.7554/eLife.18675.

Ramalho, J.S., R. Anders, G.B. Jaissle, M.W. Seeliger, C. Huxley, and M.C. Seabra. 2002. Rapid degradation of dominant-negative Rab27 proteins in vivo precludes their use in transgenic mouse models. *BMC Cell Biol*. 3:26. doi:10.1186/1471-2121-3-26.

Rebhun, J.F., A.F. Castro, and L.A. Quilliam. 2000. Identification of guanine nucleotide exchange factors (GEFs) for the Rap1 GTPase. Regulation of MR-GEF by M-Ras-GTP interaction. *J Biol Chem*. 275:34901–34908. doi:10.1074/jbc.M005327200.

Redmann, V., C.A. Lamb, S. Hwang, R.C. Orchard, S. Kim, M. Razi, A. Milam, S. Park, C.C. Yokoyama, A. Kambal, D. Kreamalmeyer, M.K. Bosch, M. Xiao, K. Green, J. Kim, S.M. Pruett-Miller, D.M. Ornitz, P.M. Allen, W.L. Beatty, R.E. Schmidt, A. DiAntonio, S.A. Tooze, and H.W. Virgin. 2016. Clec16a is Critical for

Autolysosome Function and Purkinje Cell Survival. *Sci Rep*. 6:23326. doi:10.1038/srep23326.

Ren, M., J. Zeng, C. De Lemos-Chiarandini, M. Rosenfeld, M. Adesnik, and D.D. Sabatini. 1996. In its active form, the GTP-binding protein rab8 interacts with a stress-activated protein kinase. *Proc Natl Acad Sci USA*. 93:5151–5155.

Riedel, F., A. Galindo, N. Muschalik, and S. Munro. 2017. The two TRAPP complexes of metazoans have distinct roles and act on different Rab GTPases. *J Cell Biol*. 217:601–617. doi:10.1083/jcb.201705068.

Rojas, A.M., G. Fuentes, A. Rausell, and A. Valencia. 2012. The Ras protein superfamily: evolutionary tree and role of conserved amino acids. *J Cell Biol*. 196:189–201. doi:10.1083/jcb.201103008.

Roland, J.T., L.A. Lapierre, and J.R. Goldenring. 2009. Alternative splicing in class V myosins determines association with Rab10. *J Biol Chem*. 284:1213–1223. doi:10.1074/jbc.M805957200.

Roux, K.J., D.I. Kim, M. Raida, and B. Burke. 2012. A promiscuous biotin ligase fusion protein identifies proximal and interacting proteins in mammalian cells. *J Cell Biol*. 196:801–810. doi:10.1083/jcb.201112098.

Sakaguchi, A., M. Sato, K. Sato, K. Gengyo-Ando, T. Yorimitsu, J. Nakai, T. Hara, and K. Sato. 2015. REI-1 Is a guanine nucleotide exchange factor regulating RAB-11 localization and function in *C. elegans* embryos. *Dev Cell*. 35:211–221. doi:10.1016/j.devcel.2015.09.013.

Sano, H., G.R. Peck, S. Blachon, and G.E. Lienhard. 2015. A potential link between insulin signaling and GLUT4 translocation: Association of Rab10-GTP with the exocyst subunit Exoc6/6b. *Biochem Biophys Res Commun*. 465:601–605. doi:10.1016/j.bbrc.2015.08.069.

Sato, T., T. Iwano, M. Kunii, S. Matsuda, R. Mizuguchi, Y. Jung, H. Hagiwara, Y. Yoshihara, M. Yuzaki, R. Harada, and A. Harada. 2014. Rab8a and Rab8b are essential for several apical transport pathways but insufficient for ciliogenesis. *J Cell Sci*. 127:422–431. doi:10.1242/jcs.136903.

Sato, Y., A. Yoshikawa, A. Yamagata, H. Mimura, M. Yamashita, K. Ookata, O. Nureki, K. Iwai, M. Komada, and S. Fukai. 2008. Structural basis for specific cleavage of Lys 63-linked polyubiquitin chains. *Nature*. 455:358–362. doi:10.1038/nature07254.

Sbrissa, D., O.C. Ikonomov, and A. Shisheva. 2002. Phosphatidylinositol 3-phosphate-interacting domains in PIKfyve. Binding specificity and role in PIKfyve. Endomenbrane localization. *J Biol Chem*. 277:6073–6079. doi:10.1074/jbc.M110194200.

Seaman, M.N.J., M.E. Harbour, D. Tattersall, E. Read, and N. Bright. 2009. Membrane recruitment of the cargo-selective retromer subcomplex is catalysed by the small GTPase Rab7 and inhibited by the Rab-GAP TBC1D5. *J Cell Sci*. 122:2371–2382. doi:10.1242/jcs.048686.

Sethi, N., Y. Yan, D. Quek, T. Schüpbach, and Y. Kang. 2010. Rabconnectin-3 is a

functional regulator of mammalian Notch signaling. *J Biol Chem*. 285:34757–34764. doi:10.1074/jbc.M110.158634.

Sharma, M., S.S.P. Giridharan, J. Rahajeng, N. Naslavsky, and S. Caplan. 2009. MICAL-L1 links EHD1 to tubular recycling endosomes and regulates receptor recycling. *Mol Biol Cell*. 20:5181–5194. doi:10.1091/mbc.e09-06-0535.

Shibata, S., T. Kawanai, T. Hara, A. Yamamoto, T. Chaya, Y. Tokuhara, C. Tsuji, M. Sakai, T. Tachibana, and S. Inagaki. 2016. ARHGEF10 directs the localization of Rab8 to Rab6-positive executive vesicles. *J Cell Sci*. 129:3620–3634. doi:10.1242/jcs.186817.

Shirakawa, R., S. Fukai, M. Kawato, T. Higashi, H. Kondo, T. Ikeda, E. Nakayama, K. Okawa, O. Nureki, T. Kimura, T. Kita, and H. Horiuchi. 2009. Tuberous sclerosis tumor suppressor complex-like complexes act as GTPase-activating proteins for Ral GTPases. *J Biol Chem*. 284:21580–21588. doi:10.1074/jbc.M109.012112.

Short, B., C. Preisinger, J. Schaletzky, R. Kopajtich, and F.A. Barr. 2002. The Rab6 GTPase regulates recruitment of the dynactin complex to Golgi membranes. *Curr Biol*. 12:1792–1795.

Short, B., C. Preisinger, R. Körner, R. Kopajtich, O. Byron, and F.A. Barr. 2001. A GRASP55-rab2 effector complex linking Golgi structure to membrane traffic. *J Cell Biol*. 155:877–883. doi:10.1083/jcb.200108079.

Silvius, J.R., P. Bhagatji, R. Leventis, and D. Terrone. 2006. K-ras4B and prenylated proteins lacking “second signals” associate dynamically with cellular membranes. *Mol Biol Cell*. 17:192–202. doi:10.1091/mbc.E05-05-0408.

Simonsen, A., R. Lippé, S. Christoforidis, J.M. Gaullier, A. Brech, J. Callaghan, B.H. Toh, C. Murphy, M. Zerial, and H. Stenmark. 1998. EEA1 links PI(3)K function to Rab5 regulation of endosome fusion. *Nature*. 394:494–498. doi:10.1038/28879.

Sobajima, T., S.-I. Yoshimura, T. Maeda, H. Miyata, E. Miyoshi, and A. Harada. 2018. The Rab11-binding protein RELCH/KIAA1468 controls intracellular cholesterol distribution. *J Cell Biol*. jcb.201709123. doi:10.1083/jcb.201709123.

Sowa, M.E., E.J. Bennett, S.P. Gygi, and J.W. Harper. 2009. Defining the human deubiquitinating enzyme interaction landscape. *Cell*. 138:389–403. doi:10.1016/j.cell.2009.04.042.

Steger, M., F. Diez, H.S. Dhekne, P. Lis, R.S. Nirujogi, O. Karayel, F. Tonelli, T.N. Martinez, E. Lorentzen, S.R. Pfeffer, D.R. Alessi, and M. Mann. 2017. Systematic proteomic analysis of LRRK2-mediated Rab GTPase phosphorylation establishes a connection to ciliogenesis. *eLife*. 6:e31012. doi:10.7554/eLife.31012.

Stenmark, H., R.G. Parton, O. Steele-Mortimer, A. Lütcke, J. Gruenberg, and M. Zerial. 1994. Inhibition of rab5 GTPase activity stimulates membrane fusion in endocytosis. *EMBO J*. 13:1287–1296.

Sugihara, K., S. Asano, K. Tanaka, A. Iwamatsu, K. Okawa, and Y. Ohta. 2002. The exocyst complex binds the small GTPase RalA to mediate filopodia formation. *Nat Cell Biol*. 4:73–78. doi:10.1038/ncb720.

Sumakovic, M., J. Hegermann, L. Luo, S.J. Husson, K. Schwarze, C. Olendrowitz, L. Schoofs, J. Richmond, and S. Eimer. 2009. UNC-108/RAB-2 and its effector RIC-19 are involved in dense core vesicle maturation in *Caenorhabditis elegans*. *J Cell Biol*. 186:897–914. doi:10.1083/jcb.200902096.

Sun, Y., T.T. Chiu, K.P. Foley, P.J. Bilan, and A. Klip. 2014. Myosin Va mediates Rab8A-regulated GLUT4 vesicle exocytosis in insulin-stimulated muscle cells. *Mol Biol Cell*. 25:1159–1170. doi:10.1091/mbc.E13-08-0493.

Tabata, K., K. Matsunaga, A. Sakane, T. Sasaki, T. Noda, and T. Yoshimori. 2010. Rubicon and PLEKHM1 negatively regulate the endocytic/autophagic pathway via a novel Rab7-binding domain. *Mol Biol Cell*. 21:4162–4172. doi:10.1091/mbc.E10-06-0495.

Tagaya, M., K. Arasaki, H. Inoue, and H. Kimura. 2014. Moonlighting functions of the NRZ (mammalian Dsl1) complex. *Front Cell Dev Biol*. 2:25. doi:10.3389/fcell.2014.00025.

Takai, Y., T. Sasaki, and T. Matozaki. 2001. Small GTP-binding proteins. *Physiol Rev*. 81:153–208. doi:10.1152/physrev.2001.81.1.153.

Tan, I., J. Yong, J.M. Dong, L. Lim, and T. Leung. 2008. A tripartite complex containing MRCK modulates lamellar actomyosin retrograde flow. *Cell*. 135:123–136. doi:10.1016/j.cell.2008.09.018.

Tyanova, S., T. Temu, P. Sinitcyn, A. Carlson, M.Y. Hein, T. Geiger, M. Mann, and J. Cox. 2016. The Perseus computational platform for comprehensive analysis of (prote)omics data. *Nat Meth*. 13:731–740. doi:10.1038/nmeth.3901.

Valsdottir, R., H. Hashimoto, K. Ashman, T. Koda, B. Storrie, and T. Nilsson. 2001. Identification of rabaptin-5, rabex-5, and GM130 as putative effectors of rab33b, a regulator of retrograde traffic between the Golgi apparatus and ER. *FEBS Lett*. 508:201–209.

Velthuis, te, A.J.W., and C.P. Bagowski. 2007. PDZ and LIM domain-encoding genes: molecular interactions and their role in development. *Scientific World Journal*. 7:1470–1492. doi:10.1100/tsw.2007.232.

Vetter, I.R., and A. Wittinghofer. 2001. The guanine nucleotide-binding switch in three dimensions. *Science*. 294:1299–1304. doi:10.1126/science.1062023.

Vigil, D., J. Cherfils, K.L. Rossman, and C.J. Der. 2010. Ras superfamily GEFs and GAPs: validated and tractable targets for cancer therapy? *Nat Rev Cancer*. 10:842–857. doi:10.1038/nrc2960.

Vikis, H.G., S. Stewart, and K.-L. Guan. 2002. SmgGDS displays differential binding and exchange activity towards different Ras isoforms. *Oncogene*. 21:2425–2432. doi:10.1038/sj.onc.1205306.

Wandinger-Ness, A., and M. Zerial. 2014. Rab proteins and the compartmentalization of the endosomal system. *Cold Spring Harbor Perspectives in Biology*. 6:a022616. doi:10.1101/cshperspect.a022616.

Wang, Z., G. Miao, X. Xue, X. Guo, C. Yuan, Z. Wang, G. Zhang, Y. Chen, D. Feng, J. Hu, and H. Zhang. 2016. The Vici Syndrome Protein EPG5 Is a Rab7 Effector

that Determines the Fusion Specificity of Autophagosomes with Late Endosomes/Lysosomes. *Mol Cell*. 63:781–795. doi:10.1016/j.molcel.2016.08.021.

Williams, C., R. Choudhury, E. McKenzie, and M. Lowe. 2007. Targeting of the type II inositol polyphosphate 5-phosphatase INPP5B to the early secretory pathway. *J Cell Sci*. 120:3941–3951. doi:10.1242/jcs.014423.

Xu, D., Y. Li, L. Wu, Y. Li, D. Zhao, J. Yu, T. Huang, C. Ferguson, R.G. Parton, H. Yang, and P. Li. 2018. Rab18 promotes lipid droplet (LD) growth by tethering the ER to LDs through SNARE and NRZ interactions. *J Cell Biol*. 217:975–995. doi:10.1083/jcb.201704184.

Xu, L., M.E. Sowa, J. Chen, X. Li, S.P. Gygi, and J.W. Harper. 2008. An FTS/Hook/p107(FHIP) complex interacts with and promotes endosomal clustering by the homotypic vacuolar protein sorting complex. *Mol Biol Cell*. 19:5059–5071. doi:10.1091/mbc.E08-05-0473.

Yamaguchi, A., T. Urano, T. Goi, and L.A. Feig. 1997. An Eps homology (EH) domain protein that binds to the Ral-GTPase target, RalBP1. *J Biol Chem*. 272:31230–31234.

Yan, Y., N. Denef, and T. Schüpbach. 2009. The vacuolar proton pump, V-ATPase, is required for notch signaling and endosomal trafficking in *Drosophila*. *Dev Cell*. 17:387–402. doi:10.1016/j.devcel.2009.07.001.

Yang, H., X. Jiang, B. Li, H.J. Yang, M. Miller, A. Yang, A. Dhar, and N.P. Pavletich. 2017. Mechanisms of mTORC1 activation by RHEB and inhibition by PRAS40. *Nature*. 552:368–373. doi:10.1038/nature25023.

Yin, J., Y. Huang, P. Guo, S. Hu, S. Yoshina, N. Xuan, Q. Gan, S. Mitani, C. Yang, and X. Wang. 2017. GOP-1 promotes apoptotic cell degradation by activating the small GTPase Rab2 in *C. elegans*. *J Cell Biol*. 216:1775–1794. doi:10.1083/jcb.201610001.

Zeng, J., M. Ren, D. Gravotta, C. De Lemos-Chiarandini, M. Lui, H. Erdjument-Bromage, P. Tempst, G. Xu, T.H. Shen, T. Morimoto, M. Adesnik, and D.D. Sabatini. 1999. Identification of a putative effector protein for rab11 that participates in transferrin recycling. *Proc Natl Acad Sci USA*. 96:2840–2845.

Zheng, B., T. Tang, N. Tang, K. Kudlicka, K. Ohtsubo, P. Ma, J.D. Marth, M.G. Farquhar, and E. Lehtonen. 2006. Essential role of RGS-PX1/sorting nexin 13 in mouse development and regulation of endocytosis dynamics. *Proc Natl Acad Sci USA*. 103:16776–16781. doi:10.1073/pnas.0607974103.

Zheng, J.Y., T. Koda, T. Fujiwara, M. Kishi, Y. Ikehara, and M. Kakinuma. 1998. A novel Rab GTPase, Rab33B, is ubiquitously expressed and localized to the medial Golgi cisternae. *J Cell Sci*. 111:1061–1069.

Figure Legends.

Figure 1. MitoID: Expression of BirA*-tagged GTPases on the surface of mitochondria.

(A) Schematic of the MitoID approach in which a GTPase is expressed as a chimera with BirA* and a mitochondrial targeting sequence. Also shown is the structure of a typical Ras superfamily GTPase and the of chimeric version used for MitoID.

(B) Confocal images of HeLa cells expressing mitochondrially targeted forms of Rab5A-BirA* as in (A), and stained for the HA tag in the chimera as well as markers for the mitochondria and Golgi. The Rab5A chimeras have either the Q79L or the S34N versions that lock them in the GTP- or GDP-bound states respectively.

(C) Confocal images of HeLa cells expressing mitochondrial Rab5A(Q79L)-BirA*, or untransfected, and labelled for the chimera and with biotin-binding neutravidin and a Golgi marker.

(D) As (C) except that the cells also expressed a GFP-fusion to a PX domain that binds PtdIns(3)P on endosomes. The latter are not relocated to the Rab5A(Q69L)-covered mitochondria.

(E, F). Confocal micrographs of cells expressing mitochondrial forms of Rab2A-BirA* in either the GTP-form (Q65L) or the GDP-form (S20N) and stained for mitochondria, the Golgi or with neutravidin as indicated. The Rab2A chimeras accumulate on mitochondria along with biotin, but not the Golgi markers.

Figure 2. Expression of mitochondrial Rab5A-BirA* chimeras leads to biotinylation of known Rab5A effectors and regulators.

(A) Plot of spectral counts obtained for individual proteins following mass-spectrometric analysis of streptavidin precipitations from cells expressing mitochondrial forms of Rab5A-BirA*. These forms were either GTP-bound (Q79L) or GDP-bound (S34N), and the counts represent means of triplicate biological repeats. The most abundant proteins found with both are Rab5A and the endogenous biotin-

containing proteins Acetyl-CoA carboxylase (ACACA) and pyruvate carboxylase (PC).

(B) As (A) except only the region in the dashed box in (A) is shown. Known Rab5 effectors and exchange factors are labelled as indicated by their gene names. The effectors are specific for the GTP form (Q79L), whilst the exchange factors are found with the GDP form (S34N). The proteins encoded by RABEP1 and RABGEF1 are found with both forms, but they are know to exist as a dimer that has Rab5 GEF activity but is also a Rab5 effector.

(C) Spectral counts for known Rab5 interactors obtained with the two mitochondrial forms of Rab5A shown in (A) and BirA* alone as a control. Values from three biological replicates are shown, with the area of the circle proportional to the number of counts.

Figure 3. Comparison of Rab5A MitoID data to that obtained from sixteen other GTPases.

(A) Spectral counts for the indicated proteins obtained from triple replicates of MitoID with the indicated GTPases. All GTPases are in either the GDP (D) or GTP (T) form and the proteins are ranked by their highest spectral counts with the GTP form of Rab5A (Rab5A(Q79L)). Only the top 34 proteins are shown with the full list in Supplementary file 1. Known Rab5 effectors are shown red text and Rab5A with blue.

(B) As (A) except that the spectral counts have been converted to WD scores and the proteins ranked by their highest WD score with Rab5A(Q79L). Known Rab5 effectors now dominate the highest positions in the list.

(C) Volcano plot comparing the spectral intensities from MitoID with Rab5A(Q79L) to MitoID with the GDP-bound forms of Rab5A and sixteen other GTPases (background). Known Rab5 effectors are marked red. Values are in Supplementary file 3.

(D) Bubble-volcano plot as in (C), but with the area of each point proportional to the root of the WD score. The root was used to ensure that the full range of bubble sizes was visible on the plot.

Figure 4. Application of MitoID to GTP-locked forms of Rab2A, Rab6A, Rab7A, Rab8A, Rab9A and Rab10.
(A-F). Bubble-volcano plots of MitoID with the indicated Rabs, each with a mutation predicted to lock it in the GTP-bound form. In each case the Rab is compared to a background comprising the GDP-locked/empty forms of all seventeen GTPases, with the size of the bubbles proportional to the WD scores. Indicated are known effectors (red) and GAPs (blue). The Rab is omitted and all values are in Supplementary file 3.

Figure 5. Application of MitoID to GTP-locked forms of Rab11A, Rab18, Rab30, and Rab33B.
(A-D). Bubble-volcano plots of MitoID with the GTP-locked forms of the indicated Rabs. In each case the Rab is compared to a background comprising the GDP-locked forms of all seventeen GTPases, with the size of the bubbles proportional to the WD scores. Indicated are known effectors (red) and GAPs (blue). The Rab is omitted and all values are in Supplementary file 3.

Figure 6. Application of MitoID to GDP-locked/empty forms of Rab6A, Rab2A, Rab5A, and Rab11A.
(A-D). Bubble-volcano plots of MitoID with the indicated Rabs, each with a mutation predicted to lock it in the GDP-bound form. In each case the Rab is compared to a background comprising the GDP-locked forms of seventeen GTPases, with the size of the bubbles proportional to the WD scores. Indicated are known effectors (red) and GEFs (yellow). The Rab is omitted and all values are in Supplementary file 3.

Figure 7. Validation of putative effectors for Rab2A, Rab5A and Rab9A.

(A) Affinity chromatography of cell lysates (input) using GST-fusions to the indicated GTP-locked (QL) or GDP-locked Rabs. The bound proteins were eluted and probed with antibodies to the indicated proteins. Lysates were from HEK293 cells and probed for STAMBPL1, or from rat brain and probed for ARFGEF3.
(B) Confocal micrographs of MEFs expressing either GFP-STAMPBL1 alone and probed for a Golgi marker, or co-expressing the mitochondrial Rab2A(Q65L)-BirA* as indicated.
(C) As (B) except that the cells were expressing GFP-ARFGEF3.
(D) Coomassie blue stained gel showing affinity chromatography of purified recombinant GFP-STAMBPL1 using GST fusions to the indicate GTP-locked (QL) or GDP-locked (SN) Rabs. The recombinant GFP-STAMBPL1 binds specifically to the GTP form of Rab2A.
(E) Affinity chromatography of HeLa cell lysates (input) using GST-fusions to the indicated GTP-locked (QL) or GDP-locked Rabs. The bound proteins were eluted and probed with antibodies to the indicated proteins. TBCK, OSBPL9 and RELCH show specific binding to the GTP form of Rab5, with RELCH also binding to Rab11-GTP as previously reported (Sobajima et al., 2018).
(F) Confocal micrographs of cells expressing GFP-TBCK alone, or with co-expression of mitochondrial Rab5A(Q79L)-BirA* as indicated.
(G) Coomassie blue stained gel showing affinity chromatography of lysate from E. coli expressing His_6-Nde1 using GST fusions to GTP-locked (Q66L) or GDP-locked (S21N) Rab9A. The samples were also immunoblotted for the His_6 tag. The recombinant His_6-Nde1 binds specifically to the GTP form of Rab9A.
(H) Affinity chromatography of lysate from HEK293 cells expressing FLAG-HPS3 (input) using GST-fusions to GTP-locked (QL) or GDP-locked (SN) Rab9A. The bound proteins were eluted and probed for the FLAG tag.
(I) Confocal micrographs of HeLa cells expressing FLAG-HPS3 and mitochondrial Rab9A(Q66L)-BirA* (GTP-locked) or Rab9A(S21N)-BirA* (GDP-locked). The GTP-form specifically recruits HPS3 to mitochondria.

Figure 8. Application of MitoID to N-Ras, RalB and Rheb.
(A-F). Bubble-volcano plots of MitoID with the indicated Ras family GTPases, each with mutations predicted to lock it into the GTP-bound form, with N-Ras also shown with the GDP-bound/empty form. In each case the GTPase is compared to a background comprising the GDP-locked/empty forms of seventeen GTPases, with the size of the bubbles proportional to the WD scores. Indicated are known effectors (red), GAPs (blue) and GEFS (yellow). All values are in Supplementary file 4.

Figure 9. Application of MitoID to CDC42, RhoA and Rac1.
(A-F). Bubble-volcano plots of MitoID with the indicated Rho family GTPase, each with mutations predicted to lock it in to either the GTP-bound (A,C,E), or GDP-bound/empty form (B,D,G). In each case the GTPase is compared to a background comprising the GDP-locked/empty forms of seventeen GTPases, with the size of the bubbles proportional to the WD scores. Indicated are known effectors (red), GAPs (blue) and GEFS (yellow). All values are in Supplementary file 4.

Figure 1 - Figure supplement 1. Expression of representative BirA*-tagged GTPases on the surface on mitochondria.
(A-C)) Confocal images of HeLa cells expressing mitochondrially targeted forms of the indicate GTPases, and stained for the HA tag in the chimera as well as markers for the mitochondria and Golgi.

Figure 9 - Figure supplement 1. MitoID with sequence variants of GTPases.
(A,B) Bubble-volcano plots of MitoID with the GTP-locked form of Rac1 (Q60L) or with the same GTPase from which a C-terminal stretch of six basic residues has been deleted (Δ183-188). In each case the GTPase is compared to a background comprising the GDP-locked/empty forms of seventeen GTPases. Known effectors

and GAPs are indicated along with proteins whose GO annotations include the term DNA-binding or RNA-binding. The removal of the basic stretch reduces contamination with the latter proteins.
(C) Immunoblot of strepatividin precipitates from cells in which MitoID had been performed with the indicated versions of Rab5A(Q79L). A representative lysate, and the precipitates were blotted for the indicated Rab5 effectors. Mutation of Ser84 reduces biotinylation of OSBPL9, but has no effect on that of two other effectors, EEA1 and PIK3R4.

Additional files

Supplementary file 1. Analysis of mass-spectral data from GTPase MitoID based on spectral counts.
Proteins identified by MitoID with at least one GTPase. Total spectral counts for biological triplicates of GTP-bound (T) and GDP-bound forms (D) are in Sheet S1A. Spectral counts were converted into D scores and WD scores based on the CompPASS platform. D scores in Sheet S1B, mean D scores in Sheet S1C, WD scores in Sheet S1D and mean WD scores in Sheet S1E (see tabs at bottom of sheet). Excel (.xlsx) file.

Supplementary file 2. Analysis of mass-spectral data from GTPase MitoID based on peak intensities.
Label free quantitation (LFQ) intensities from MaxQuant are shown for all proteins identified by MitoID with at least one GTPase. Excel (.xlsx) file.

Supplementary file 3. Volcano plot data from mass spectral peak intensities from MitoID with GTPases of the Rab family.
For each Rab form indicated in the tabs, the LFQ intensities of every protein found in at least two of the triplicates was compared to the values obtained with the GDP

forms of all GTPases by using the Perseus platform. The difference, expressed as log_2 of the ratio, and the P-value for the significance of the difference are shown, with these being used to generate the volcano plots shown in the figures. Also shown are the WD score for each interaction as obtained from analysis of spectral counts. Excel (.xlsx) file.

Supplementary file 4. Volcano plot data from mass spectral peak intensities from MitoID with GTPases of the Rho and Ras families.
For each GTPase form indicated in the tabs, the LFQ intensities of every protein found in at least two of the triplicates was compared to the values obtained with the GDP forms of all GTPases by using the Perseus platform. The difference, expressed as log_2 of the ratio, and the P-value for the significance of the difference are shown, with these being used to generate the volcano plots shown in the figures. Also shown are the WD score for each interaction as obtained from analysis of spectral counts. Excel (.xlsx) file.

Figure 1

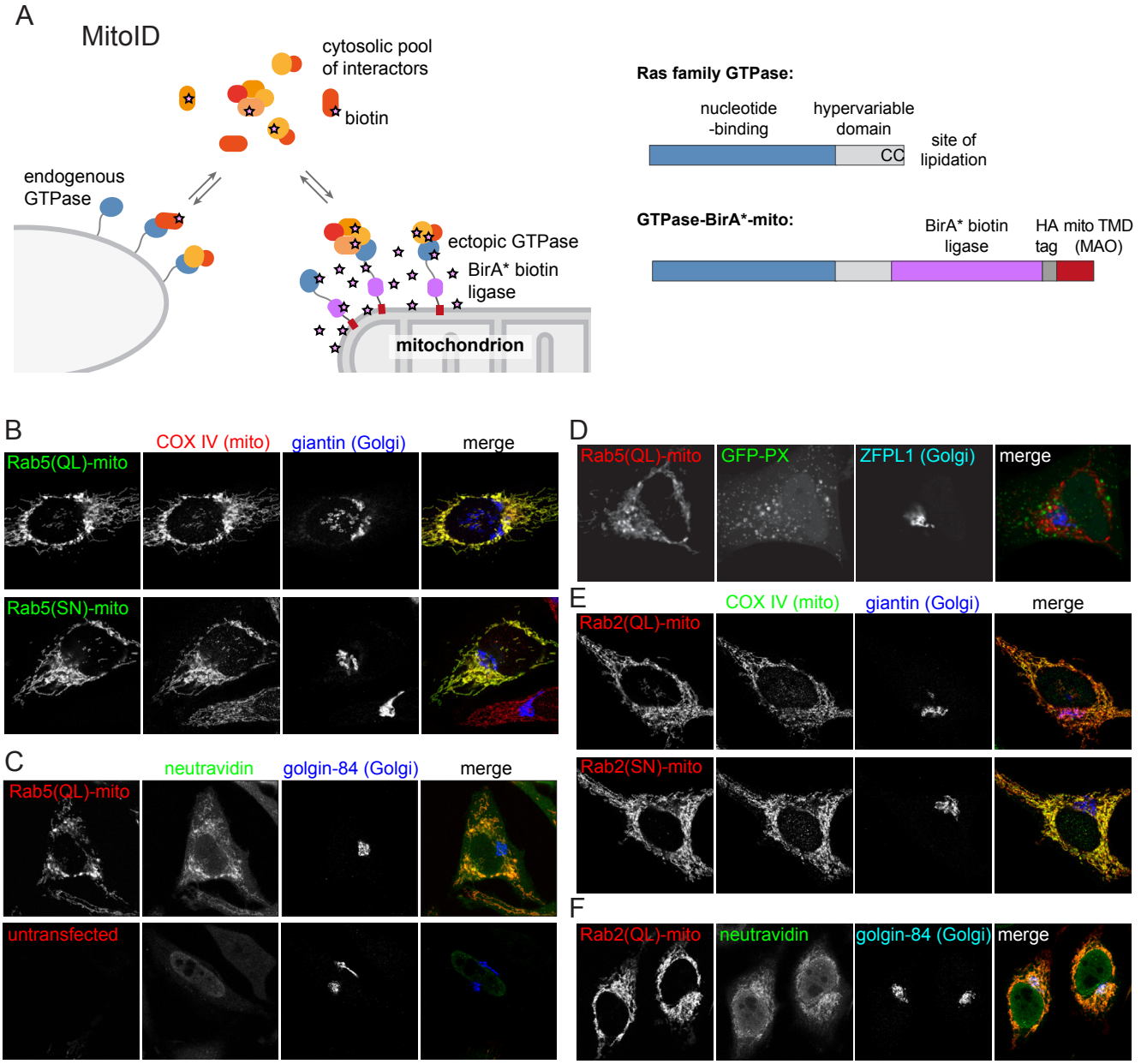
A
MitoID
cytosolic pool
of interactors
biotin
endogenous
GTPase
ectopic GTPase
BirA* biotin
ligase
mitochondrion
Ras family GTPase:
nucleotide
-binding
hypervariable
domain
CC
site of
lipidation
GTPase-BirA*-mito:
BirA* biotin
ligase
HA
tag
mito TMD
(MAO)
B
COX IV (mito)
giantin (Golgi)
merge
Rab5(QL)-mito
Rab5(SN)-mito
C
neutravidin
golgin-84 (Golgi)
merge
Rab5(QL)-mito
untransfected
D
Rab5(QL)-mito
GFP-PX
ZFPL1 (Golgi)
merge
E
COX IV (mito)
giantin (Golgi)
merge
Rab2(QL)-mito
Rab2(SN)-mito
F
Rab2(QL)-mito
neutravidin
golgin-84 (Golgi)
merge

Figure 2

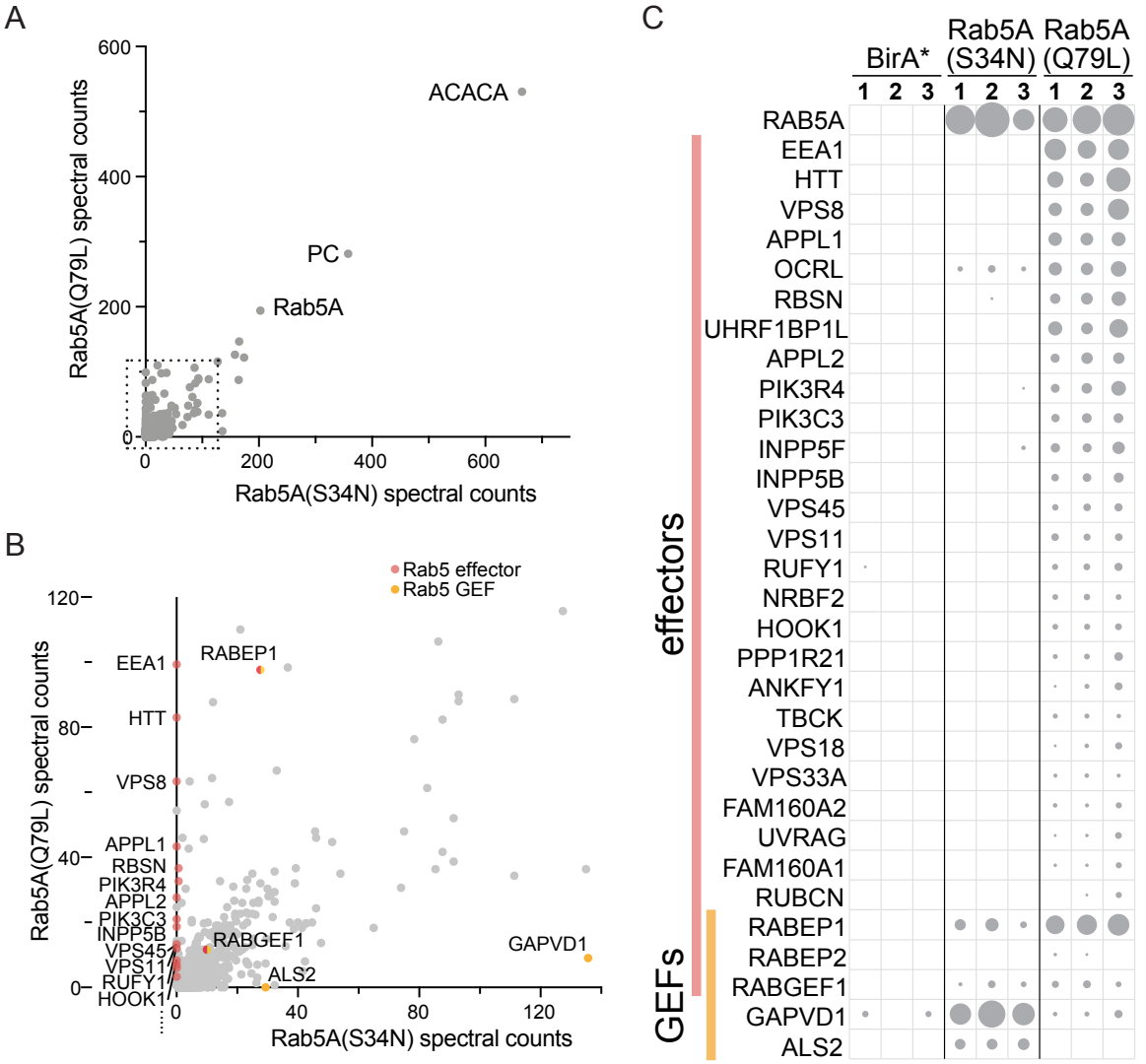
A
Rab5A(Q79L) spectral counts
Rab5A(S34N) spectral counts
ACACA
PC
Rab5A
B
Rab5 effector
Rab5 GEF
Rab5A(Q79L) spectral counts
Rab5A(S34N) spectral counts
EEA1
HTT
VPS8
APPL1
RBSN
PIK3R4
APPL2
PIK3C3
INPP5B
VPS45
VPS11
RUFY1
HOOK1
RABEP1
RABGEF1
ALS2
GAPVD1
C
BirA*
Rab5A (S34N)
Rab5A (Q79L)
1 2 3 1 2 3 1 2 3
effectors
GEFs
RAB5A
EEA1
HTT
VPS8
APPL1
OCRL
RBSN
UHRF1BP1L
APPL2
PIK3R4
PIK3C3
INPP5F
INPP5B
VPS45
VPS11
RUFY1
NRBF2
HOOK1
PPP1R21
ANKFY1
TBCK
VPS18
VPS33A
FAM160A2
UVRAG
FAM160A1
RUBCN
RABEP1
RABEP2
RABGEF1
GAPVD1
ALS2

Figure 3

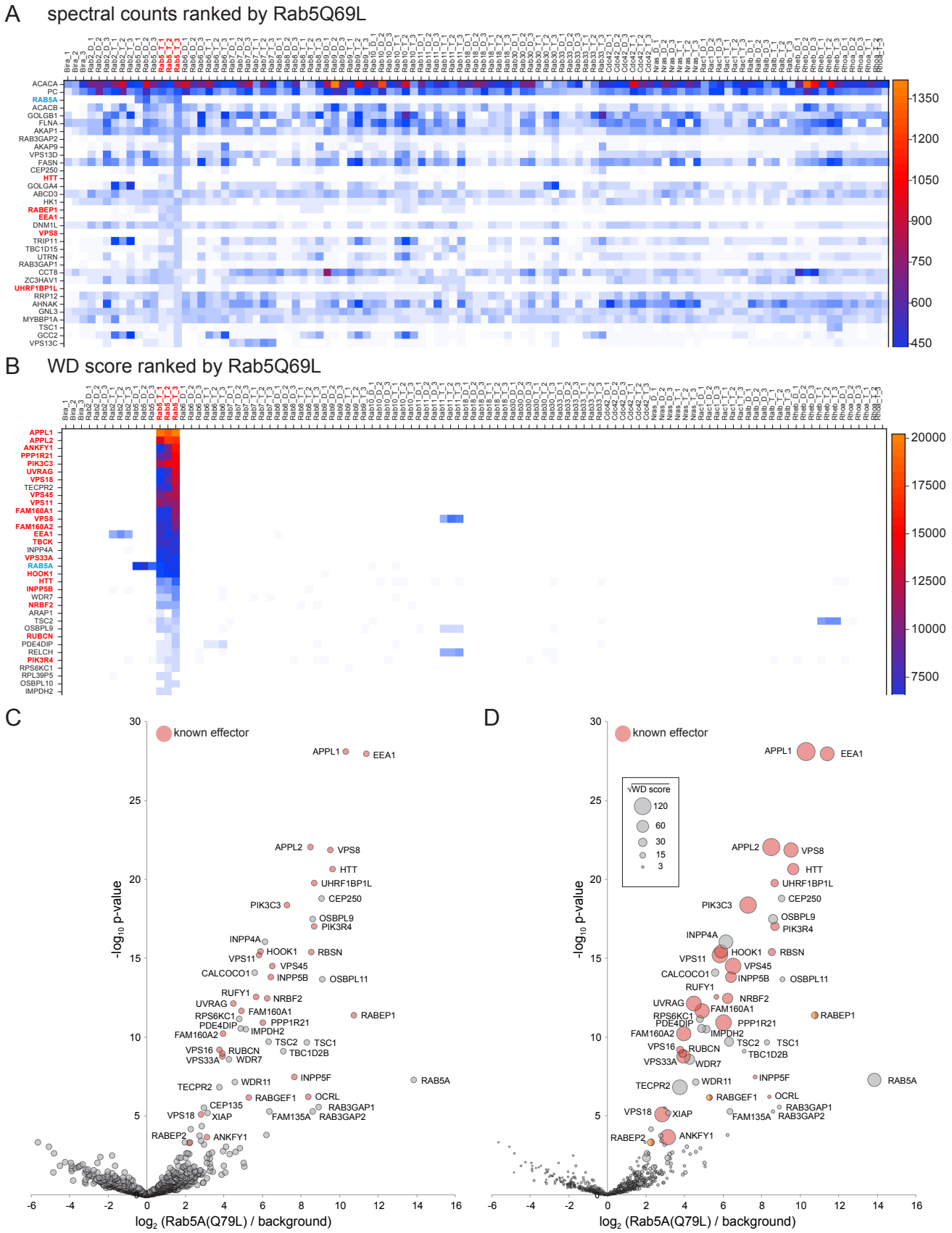
A spectral counts ranked by Rab5Q69L
B WD score ranked by Rab5Q69L
C
D
known effector
-log10 p-value
log2 (Rab5A(Q79L) / background)
√WD score
120
60
30
15
3
APPL1
EEA1
APPL2
VPS8
HTT
UHRF1BP1L
CEP250
PIK3C3
OSBPL9
PIK3R4
INPP4A
HOOK1
RBSN
VPS11
VPS45
CALCOCO1
INPP5B
OSBPL11
RUFY1
NRBF2
UVRAG
FAM160A1
RPS6KC1
PPP1R21
PDE4DIP
IMPDH2
FAM160A2
TSC2
TSC1
VPS16
RUBCN
TBC1D2B
VPS33A
WDR7
RABEP1
INPP5F
RAB5A
TECPR2
WDR11
RABGEF1
OCRL
CEP135
RAB3GAP1
VPS18
XIAP
FAM135A
RAB3GAP2
RABEP2
ANKFY1

Figure 4

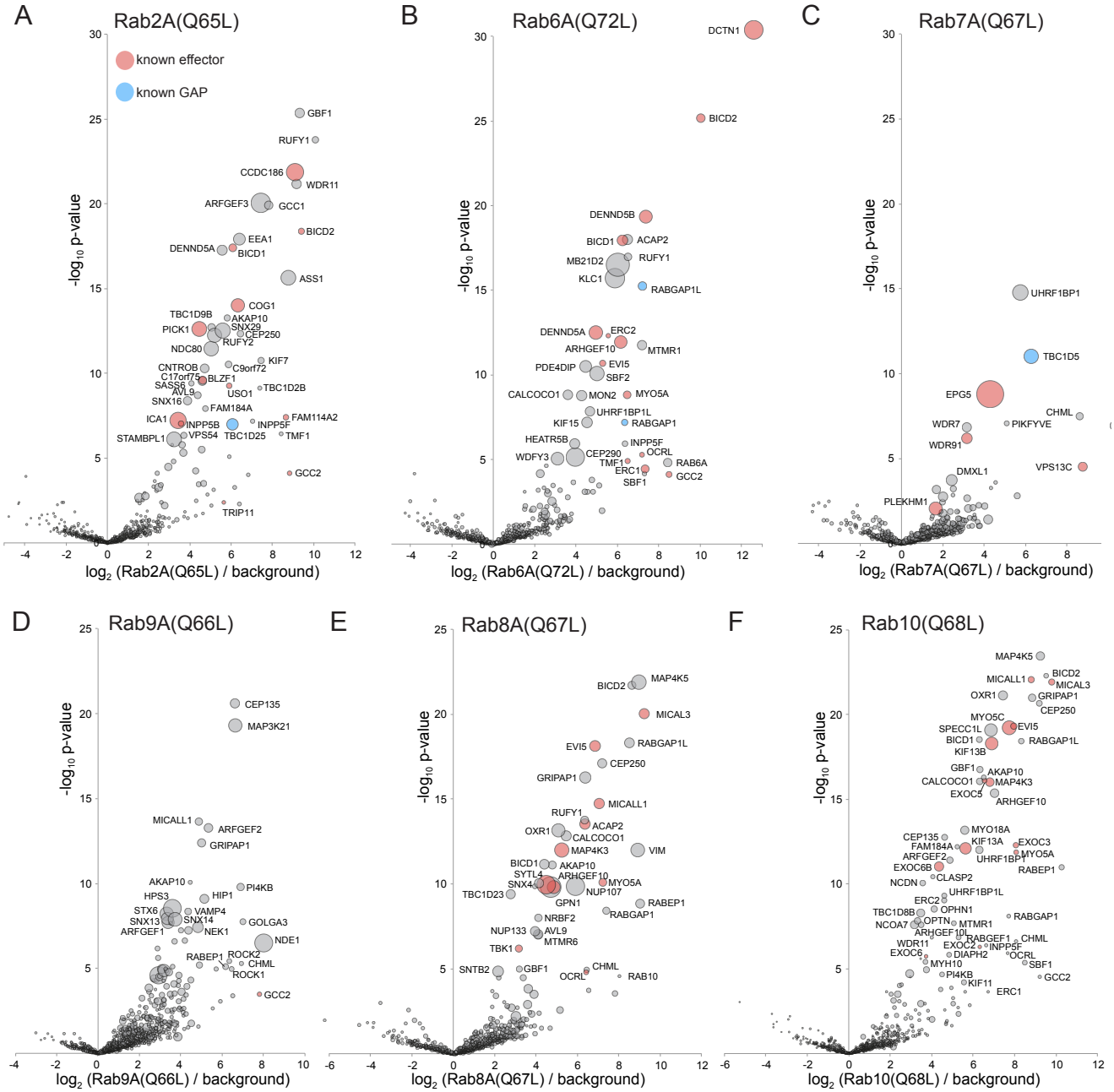
A
Rab2A(Q65L)
known effector
known GAP
-log10 p-value
log2 (Rab2A(Q65L) / background)
GBF1
RUFY1
CCDC186
WDR11
ARFGEF3
GCC1
BICD2
EEA1
DENND5A
BICD1
ASS1
COG1
TBC1D9B
AKAP10
PICK1
SNX29
CEP250
RUFY2
NDC80
KIF7
CNTROB
C9orf72
C17orf75
BLZF1
SASS6
AVL9
USO1
TBC1D2B
SNX16
FAM184A
ICA1
INPP5B
INPP5F
FAM114A2
STAMBPL1
VPS54
TBC1D25
TMF1
GCC2
TRIP11
B
Rab6A(Q72L)
DCTN1
BICD2
DENND5B
BICD1
ACAP2
MB21D2
RUFY1
KLC1
RABGAP1L
DENND5A
ERC2
ARHGEF10
MTMR1
PDE4DIP
EVI5
SBF2
CALCOCO1
MON2
MYO5A
UHRF1BP1L
KIF15
RABGAP1
HEATR5B
INPP5F
WDFY3
CEP290
OCRL
TMF1
RAB6A
ERC1
GCC2
SBF1
C
Rab7A(Q67L)
UHRF1BP1
TBC1D5
EPG5
CHML
WDR7
PIKFYVE
WDR91
VPS13C
DMXL1
PLEKHM1
D
Rab9A(Q66L)
CEP135
MAP3K21
MICALL1
ARFGEF2
GRIPAP1
AKAP10
PI4KB
HPS3
HIP1
STX6
VAMP4
SNX13
SNX14
GOLGA3
ARFGEF1
NEK1
NDE1
RABEP1
ROCK2
CHML
ROCK1
GCC2
E
Rab8A(Q67L)
MAP4K5
BICD2
MICAL3
EVI5
RABGAP1L
CEP250
GRIPAP1
MICALL1
RUFY1
ACAP2
OXR1
CALCOCO1
MAP4K3
VIM
BICD1
AKAP10
SYTL4
ARHGEF10
SNX4
MYO5A
TBC1D23
NUP107
GPN1
RABEP1
RABGAP1
NRBF2
NUP133
AVL9
MTMR6
TBK1
SNTB2
GBF1
CHML
OCRL
RAB10
F
Rab10(Q68L)
MAP4K5
MICALL1
BICD2
MICAL3
OXR1
GRIPAP1
CEP250
MYO5C
SPECC1L
EVI5
BICD1
RABGAP1L
KIF13B
GBF1
AKAP10
CALCOCO1
MAP4K3
EXOC5
ARHGEF10
MYO18A
CEP135
KIF13A
EXOC3
FAM184A
ARFGEF2
MYO5A
UHRF1BP1
EXOC6B
RABEP1
NCDN
CLASP2
UHRF1BP1L
ERC2
TBC1D8B
OPHN1
RABGAP1
NCOA7
OPTN
MTMR1
ARHGEF10L
WDR11
RABGEF1
CHML
EXOC6
EXOC2
INPP5F
DIAPH2
OCRL
MYH10
SBF1
PI4KB
GCC2
KIF11
ERC1

Figure 5

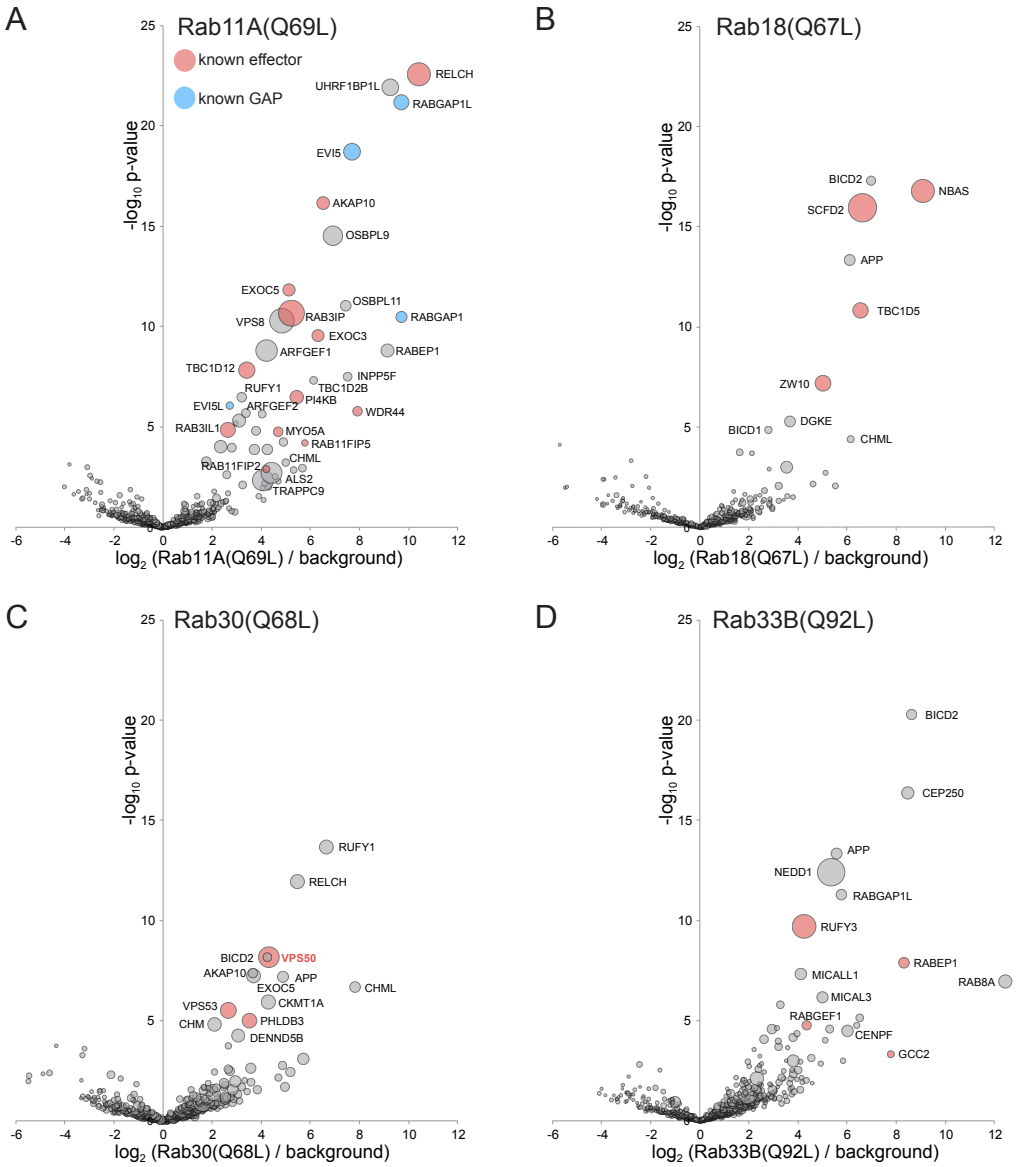
A
Rab11A(Q69L)
known effector
known GAP
RELCH
UHRF1BP1L
RABGAP1L
EVI5
AKAP10
OSBPL9
EXOC5
OSBPL11
RAB3IP
RABGAP1
VPS8
EXOC3
ARFGEF1
RABEP1
TBC1D12
INPP5F
RUFY1
TBC1D2B
PI4KB
EVI5L
ARFGEF2
WDR44
RAB3IL1
MYO5A
RAB11FIP5
CHML
RAB11FIP2
ALS2
TRAPPC9
-log10 p-value
log2 (Rab11A(Q69L) / background)
B
Rab18(Q67L)
BICD2
NBAS
SCFD2
APP
TBC1D5
ZW10
DGKE
BICD1
CHML
-log10 p-value
log2 (Rab18(Q67L) / background)
C
Rab30(Q68L)
RUFY1
RELCH
BICD2
VPS50
AKAP10
APP
EXOC5
CHML
CKMT1A
VPS53
PHLDB3
CHM
DENND5B
-log10 p-value
log2 (Rab30(Q68L) / background)
D
Rab33B(Q92L)
BICD2
CEP250
APP
NEDD1
RABGAP1L
RUFY3
RABEP1
MICALL1
RAB8A
MICAL3
RABGEF1
CENPF
GCC2
-log10 p-value
log2 (Rab33B(Q92L) / background)

Figure 6

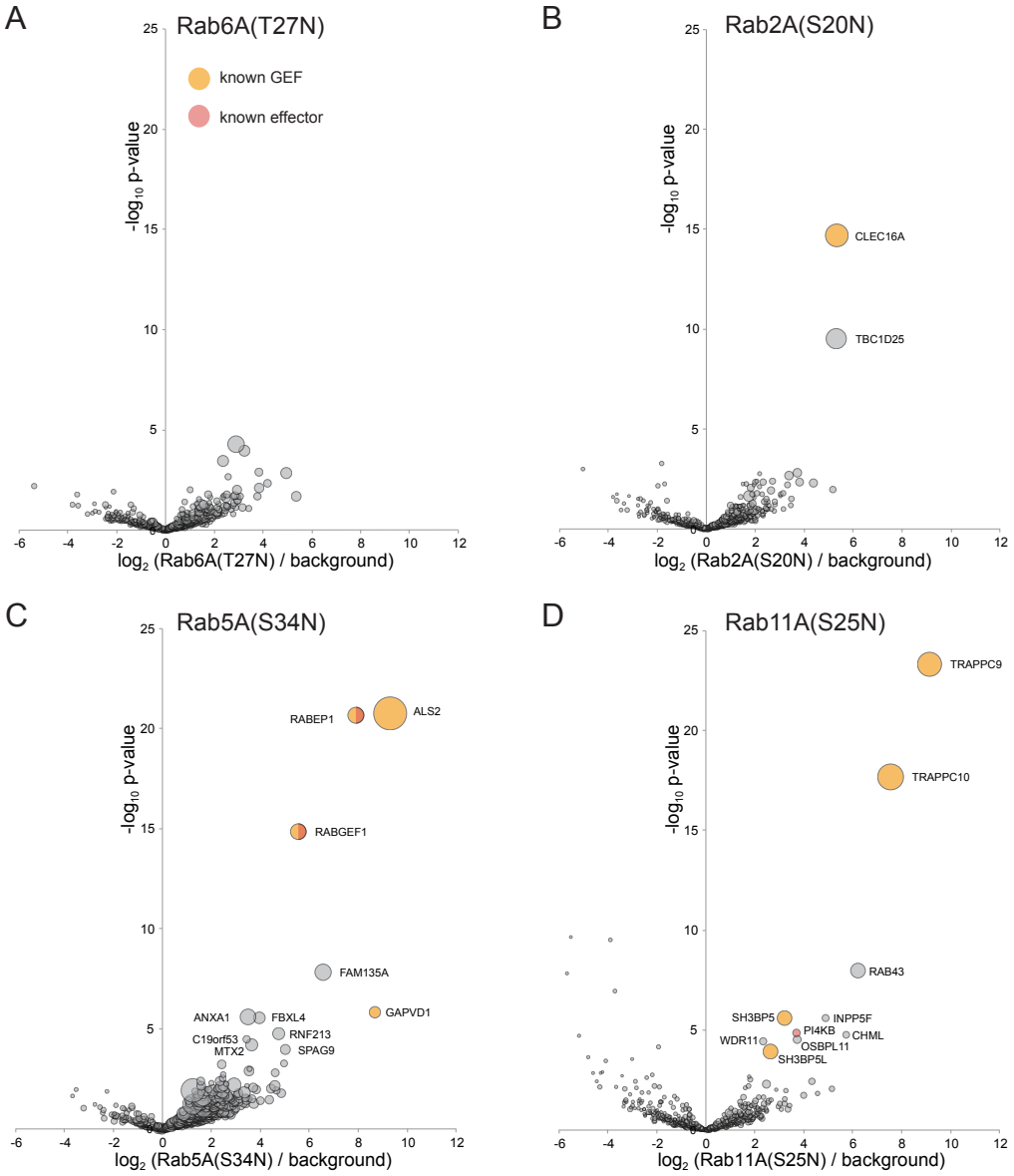
A
Rab6A(T27N)
known GEF
known effector
-log10 p-value
log2 (Rab6A(T27N) / background)
B
Rab2A(S20N)
CLEC16A
TBC1D25
-log10 p-value
log2 (Rab2A(S20N) / background)
C
Rab5A(S34N)
RABEP1
ALS2
RABGEF1
FAM135A
GAPVD1
ANXA1
FBXL4
C19orf53
RNF213
MTX2
SPAG9
-log10 p-value
log2 (Rab5A(S34N) / background)
D
Rab11A(S25N)
TRAPPC9
TRAPPC10
RAB43
SH3BP5
INPP5F
PI4KB
CHML
WDR11
OSBPL11
SH3BP5L
-log10 p-value
log2 (Rab11A(S25N) / background)

Figure 7

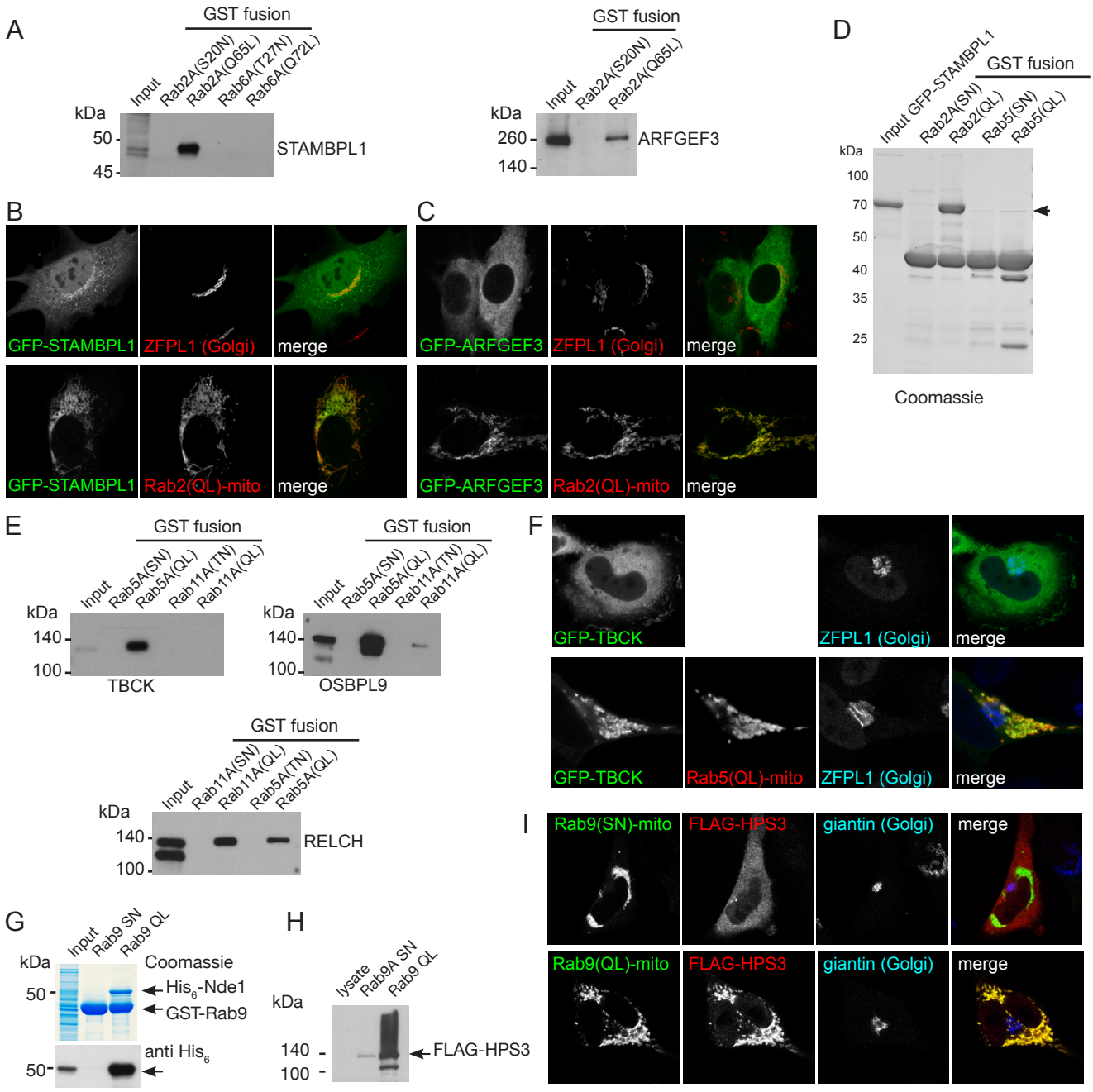
A
GST fusion
Input
Rab2A(S20N)
Rab2A(Q65L)
Rab6A(T27N)
Rab6A(Q72L)
kDa
50
45
STAMBPL1
GST fusion
Input
Rab2A(S20N)
Rab2A(Q65L)
kDa
260
140
ARFGEF3
D
Input GFP-STAMBPL1
GST fusion
Rab2A(SN)
Rab2(QL)
Rab5(SN)
Rab5(QL)
kDa
100
70
50
40
35
25
Coomassie
B
GFP-STAMBPL1
ZFPL1 (Golgi)
merge
GFP-STAMBPL1
Rab2(QL)-mito
merge
C
GFP-ARFGEF3
ZFPL1 (Golgi)
merge
GFP-ARFGEF3
Rab2(QL)-mito
merge
E
GST fusion
Input
Rab5A(SN)
Rab5A(QL)
Rab11A(TN)
Rab11A(QL)
kDa
140
100
TBCK
GST fusion
Input
Rab5A(SN)
Rab5A(QL)
Rab11A(TN)
Rab11A(QL)
kDa
140
100
OSBPL9
GST fusion
Input
Rab11A(SN)
Rab11A(QL)
Rab5A(TN)
Rab5A(QL)
kDa
140
100
RELCH
F
GFP-TBCK
ZFPL1 (Golgi)
merge
GFP-TBCK
Rab5(QL)-mito
ZFPL1 (Golgi)
merge
G
Input
Rab9 SN
Rab9 QL
kDa
Coomassie
50
His6-Nde1
GST-Rab9
anti His6
50
H
lysate
Rab9A SN
Rab9 QL
kDa
140
100
FLAG-HPS3
I
Rab9(SN)-mito
FLAG-HPS3
giantin (Golgi)
merge
Rab9(QL)-mito
FLAG-HPS3
giantin (Golgi)
merge

Figure 8

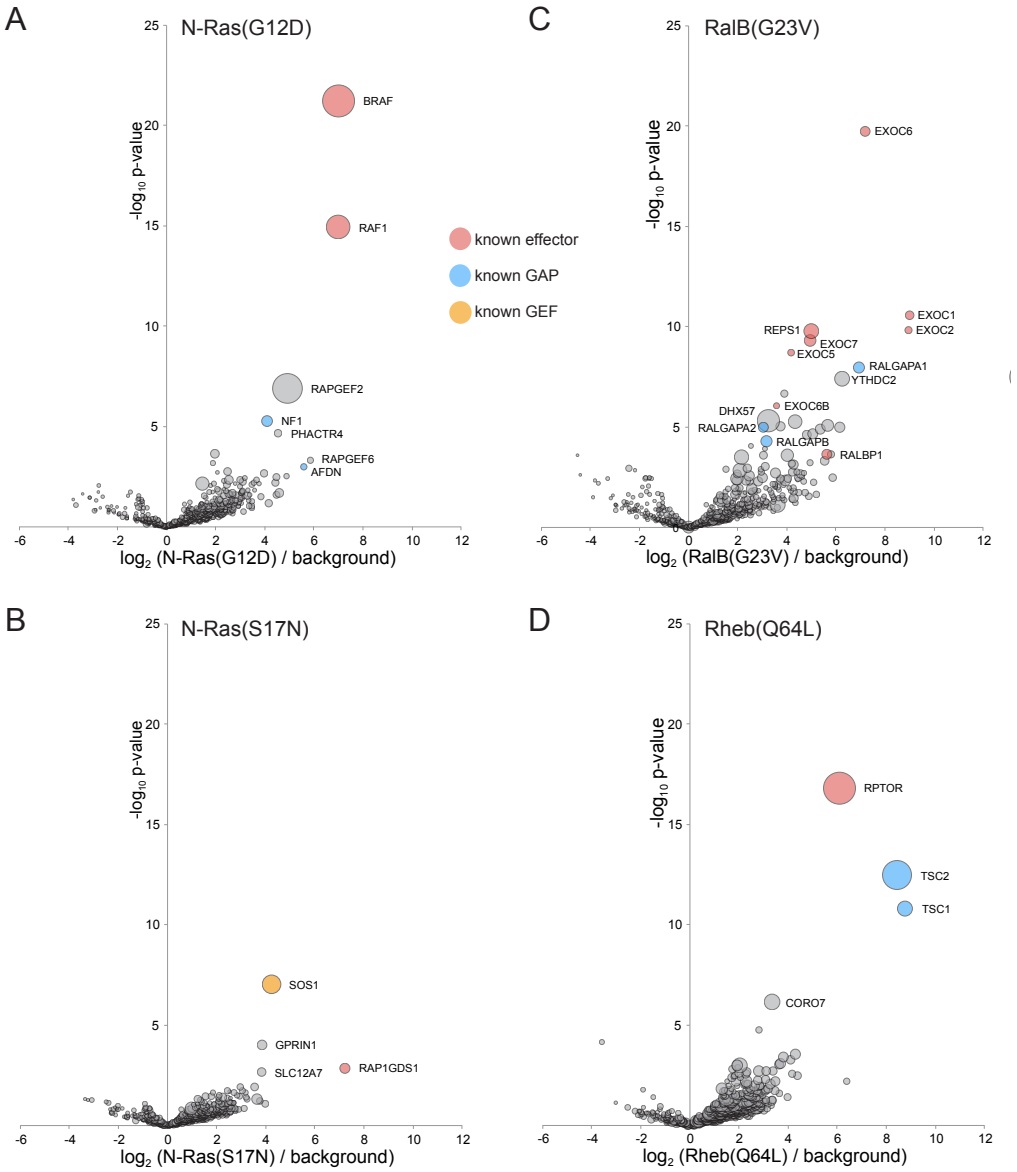
A
N-Ras(G12D)
BRAF
RAF1
RAPGEF2
NF1
PHACTR4
RAPGEF6
AFDN
-log10 p-value
log2 (N-Ras(G12D) / background)
known effector
known GAP
known GEF
C
RalB(G23V)
EXOC6
EXOC1
EXOC2
REPS1
EXOC7
EXOC5
RALGAPA1
YTHDC2
EXOC6B
DHX57
RALGAPA2
RALGAPB
RALBP1
log2 (RalB(G23V) / background)
B
N-Ras(S17N)
SOS1
GPRIN1
SLC12A7
RAP1GDS1
log2 (N-Ras(S17N) / background)
D
Rheb(Q64L)
RPTOR
TSC2
TSC1
CORO7
log2 (Rheb(Q64L) / background)

Figure 9

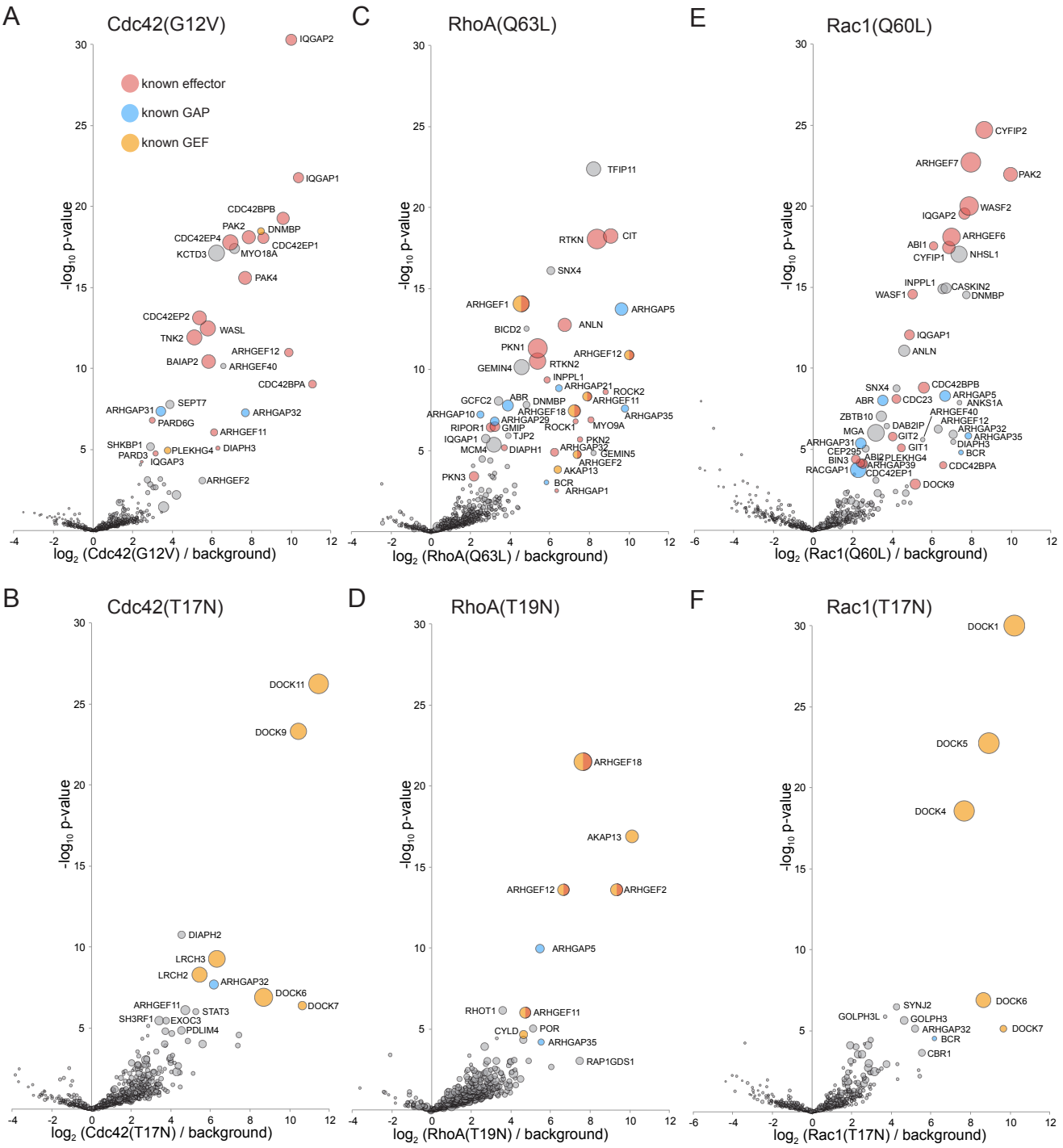
A
Cdc42(G12V)
known effector
known GAP
known GEF
IQGAP2
IQGAP1
CDC42BPB
PAK2
DNMBP
CDC42EP4
CDC42EP1
KCTD3
MYO18A
PAK4
CDC42EP2
WASL
TNK2
ARHGEF12
BAIAP2
ARHGEF40
CDC42BPA
SEPT7
ARHGAP31
ARHGAP32
PARD6G
ARHGEF11
SHKBP1
PLEKHG4
DIAPH3
PARD3
IQGAP3
ARHGEF2
-log10 p-value
log2 (Cdc42(G12V) / background)
C
RhoA(Q63L)
TFIP11
RTKN
CIT
SNX4
ARHGEF1
ARHGAP5
BICD2
ANLN
PKN1
ARHGEF12
RTKN2
GEMIN4
INPPL1
ARHGAP21
ROCK2
GCFC2
ABR
DNMBP
ARHGEF11
ARHGAP10
ARHGEF18
ARHGAP35
ARHGAP29
RIPOR1
GMIP
ROCK1
MYO9A
IQGAP1
TJP2
PKN2
MCM4
DIAPH1
ARHGAP22
GEMIN5
ARHGEF2
AKAP13
PKN3
BCR
ARHGAP1
-log10 p-value
log2 (RhoA(Q63L) / background)
E
Rac1(Q60L)
CYFIP2
ARHGEF7
PAK2
WASF2
IQGAP2
ARHGEF6
ABI1
CYFIP1
NHSL1
INPPL1
CASKIN2
WASF1
DNMBP
IQGAP1
ANLN
SNX4
CDC42BPB
ARHGAP5
ABR
CDC23
ANKS1A
ARHGEF40
ZBTB10
ARHGEF12
DAB2IP
ARHGAP32
MGA
GIT2
ARHGAP35
ARHGAP31
GIT1
DIAPH3
CEP295
BCR
ABI2
PLEKHG4
BIN3
ARHGAP39
CDC42BPA
RACGAP1
CDC42EP1
DOCK9
-log10 p-value
log2 (Rac1(Q60L) / background)
B
Cdc42(T17N)
DOCK11
DOCK9
DIAPH2
LRCH3
LRCH2
ARHGAP32
DOCK6
DOCK7
ARHGEF11
STAT3
SH3RF1
EXOC3
PDLIM4
-log10 p-value
log2 (Cdc42(T17N) / background)
D
RhoA(T19N)
ARHGEF18
AKAP13
ARHGEF12
ARHGEF2
ARHGAP5
RHOT1
ARHGEF11
CYLD
POR
ARHGAP35
RAP1GDS1
-log10 p-value
log2 (RhoA(T19N) / background)
F
Rac1(T17N)
DOCK1
DOCK5
DOCK4
DOCK6
SYNJ2
GOLPH3L
GOLPH3
ARHGAP32
DOCK7
BCR
CBR1
-log10 p-value
log2 (Rac1(T17N) / background)

Figure 1 - figure supplement 1

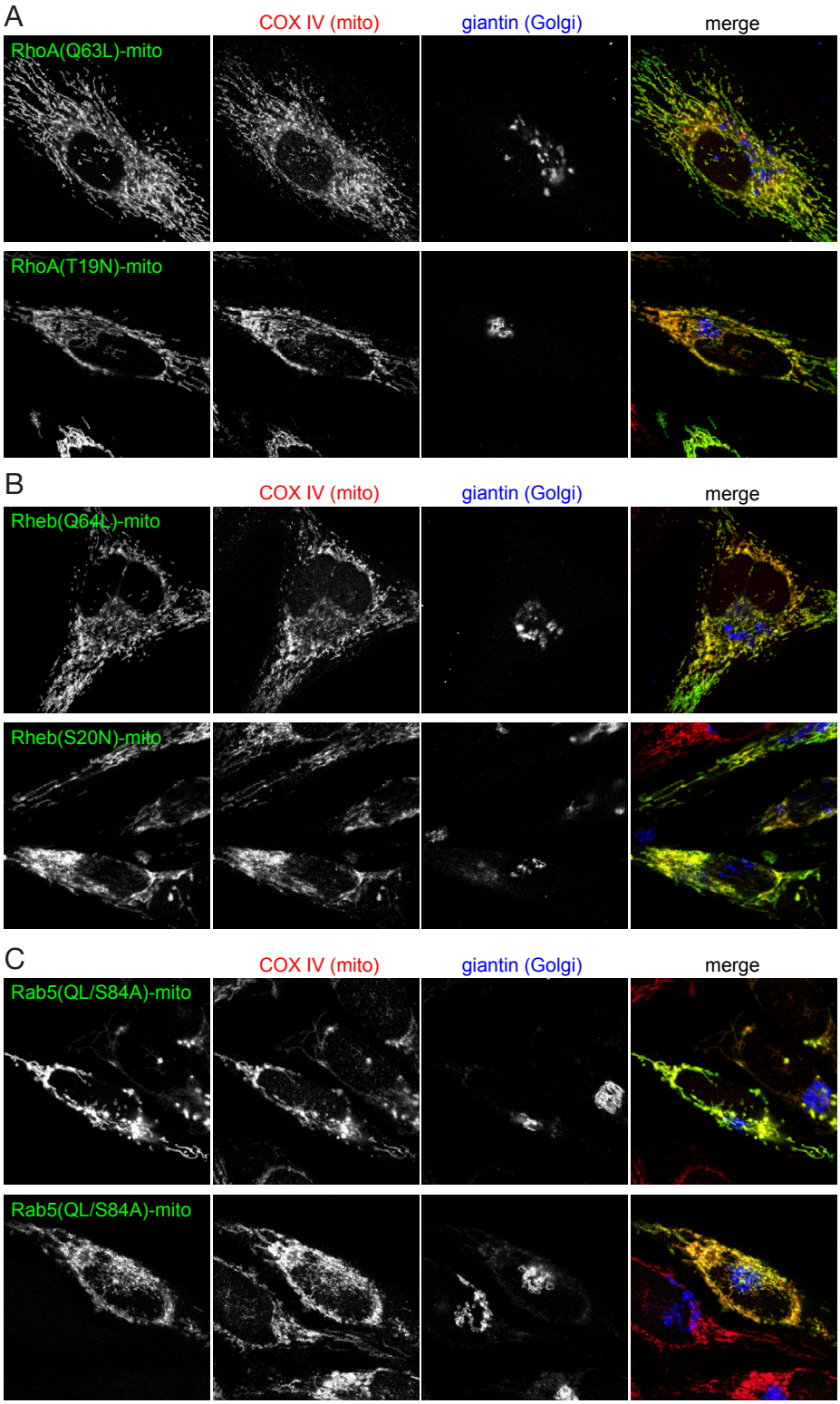
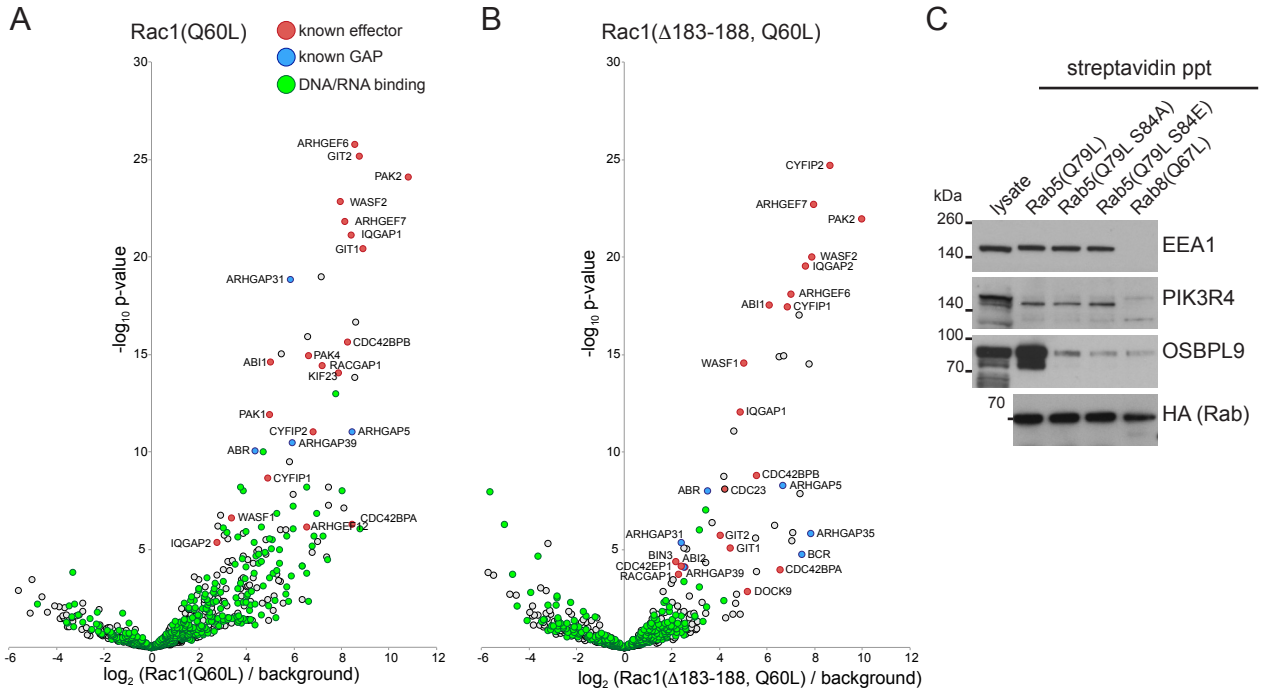
Figure 9 - figure supplement 1